FIRST-PRINCIPLES CALCULATIONS OF ORGANIC MOLECULES ADSORPTION IN NANOSTRUCTURES

By

Helena Estefanía López Avilés

In partial fulfillment of the requirements
for the degree of
MASTER OF SCIENCE (OPTICS)

PHOTONICS DIVISION,
CENTRO DE INVESTIGACIONES EN ÓPTICA, A.C.
LEÓN, GUANAJUATO, MÉXICO.

2013

Advisor: Dr. Raúl Alfonso Vázquez Nava

Evaluation Committee: Dr. Gregorio Hernández Cocoletzi

Dr. Rafael Espinosa Luna

Table of Contents

List of Tables

List of Figures

Abstract

First-principles calculations are a research field that allow to solve quantum mechanics equations without using approximate parameters, except for those inherent to numerical algorithms. These calculations are used to obtain theoretically some properties of nanometric structures, like ground-state energies and binding energies with high accuracy.

In this work we have presented the results of the interaction between some organic molecules inside a Boron Nitride Nanotube (BNNT). The organic molecules chosen are three amino acids and five nitrogenous bases: glycine, serine, cysteine, cytosine, thymine, uracil, adenine and guanine. The nanotube chosen is a zigzag (12,0) single-walled BNNT. The ground-state energies and the binding energies were obtained using three different approximations: Hartree-Fock, Density Functional Theory (DFT), and DFT-D3, the latter approach was used to take into account the dispersion interactions not present in DFT calculations. The functional used was Becke's hybrid functional with three parameters and Lee-Yang-Parr (B3LYP), which has been proved to be a good choice for this nanotube because of the agreement with experimental results. In the case of Hartree-Fock approximation, the Basis Set Superposition Error (BSSE) was calculated, because of the error of using a truncated basis set (6-31G). The results show that there is physisorption, i.e., the interaction between the BNNT and the organic molecules is dominated by the van der Waals (vdW) forces. Also, the Density Of States (DOS) was computed and it confirms that there is not chemical adsorption of the molecules inside the BNNT.

The computational calculations were developed by using free software licence like: MacMolPlt and Avogadro for build the structures and display the optimized geometries, and GAMESS for geometry optimization and DOS computation.

Acknowledgments

I would like to thank my family for all their love and support during my master degree studies.

To my colleagues and friends in this two years, specially Francisco Arteaga for all his support and advice.

To my advisor Dr. Raúl Alfonso Vázquez Nava for his guide, patience, help and wisdom that made possible to achieve this work. Also, I would like to thank Dr. Miguel Torres-Cisneros for his support since my bachelor degree.

Finally, I thank Centro de Investigaciones en Óptica and CONACYT for give me the opportunity to continue with my graduate studies. Particularly, I thank CONACYT project through Contract Number 153930.

1 Introduction

Nanotechnology is the ability to observe, measure, manipulate, and manufacture nanoscale objects (atoms and molecules). It is not merely the study of small objects, is the research and development of materials, devices, and systems that exhibit physical, chemical, and biological properties. These properties can be different from those found at larger scales. So, nanotechnology is one of the fastest growing areas in materials and engineering science and biotechnology.

One of the important research areas of nanotechnology are nanotubes, they can be used in novel physical, chemical, electronical, and medical applications, due to their thermal, electrical and mechanical properties. Particularly, Boron Nitride Nanotubes (BNNTs) have recently been studied theoretically and experimentally because of their potential medical applications as targeted drug delivery, due to their unique properties.

1.1 Boron Nitride Nanotubes (BNNTs)

Boron Nitride (BN) is known to exist in three different crystals structures, namely hexagonal BN (h-BN), cubic BN (c-BN), and wurzite BN (w-BN) as show in Fig. 1.1. Among these structures, h-BN is the stable one at room temperature and ambient pressure. It consists of stacked BN layers with a honeycomb structure. BN nanostructures ranging from single and multiwall nanotubes to BN fullerens and nanocones can be considered as having been tailored from a single BN sheet. The partially ionic character of the BN bond results in a wide band gap of about 6.5 eV for bulk h-BN.

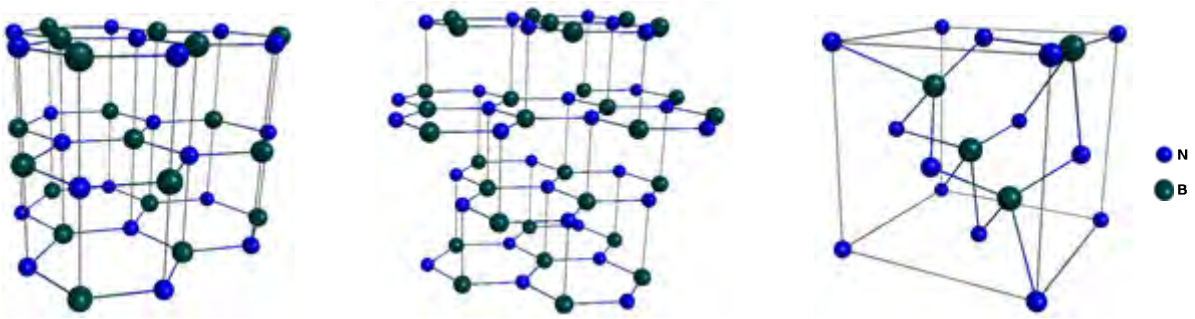

(a) (b) (c)

Figure 1.1: Boron nitride crystal structures: (a) hexagonal BN, (b) wurzite BN, (c) cubic BN.

As mentioned before, BNNTs can be considered as a layer of BN sheet rolled up into a cylinder, and the structure of a BNNT is completely specified by the chiral vector which is given in terms of a pair of integers (n, m). The chirality of BNNT do not has a significant role in determining their electrical properties [1]. The nanoscaled BN with a perfect tubular structure was first predicted theoretically in 1994 [2, 3], and then experimentally synthesized by arc-discharge in 1995 [4]. BNNTs are clasified into three types, namely, armchair (n, n) nanotubes, zigzag $(n, 0)$ nanotubes and chiral (n, m) nanotubes with $n \neq m$, see Fig. 1.2.

The smallest stable BNNT, from the energy point of view, is a (5,0) zigzag BNNT as documented by first-principles calculations [5] with a diameter of about 4.0 Å.

1.2 Properties of BNNTs

Electronic Properties

The electronic properties of BNNTs are different from those of Carbon nanotubes (CNTs). CNTs are either metallic or semi-conductive. However, with a constant wide band gap at 5.0-6.0 eV [1], which is independent of the diameter and chirality of the nanotube, unmodified BNNTs can be considered as insulating materials. Zigzag BNNTs with chirality (n,0) are expected to have direct band gap, but armchair BNNTs with chiral vectors (n,n) will have indirect band gap.

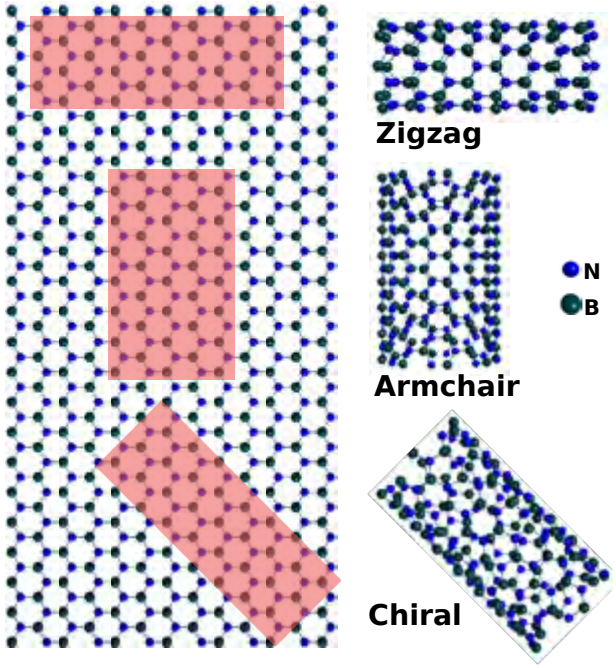

Figure 1.2: Structures of BNNTs.

The band gaps of BNNTs are tunable by doping with carbon [6], radial deformation [7], or by applying a transverse electric field across the BNNTs (giant Stark effect) [8–10]. Theoretical band structure calculations suggested that BNNTs can either be p-type or n-type semiconductors by controlling the composition of carbon into BNNTs [6]. First-principles pseudopotential density-functional calculations predicted the band-gap modification by radial deformation in BNNTs. In zigzag BNNTs, radial deformations due to transverse pressures of about 10 GPa decrease the direct band gap from 5 to 2 eV, allowing for optical applications in the visible range. However, the band gaps of armchair BNNTs are found to be insensitive to radial deformations. Finally, by applying transverse electric fields the band gap of BNNTs can be reduced and even completely removed. The giant Stark effect has been observed experimentally when applying a Scanning Tunneling Microscopy (STM) tip to impose a local transverse electric field on BNNTs and simultaneously probing the electronic properties [10].

Mechanical Properties

The elastic properties of BNNTs have theoretically been investigated. The Young modulus of BNNTs was calculated using a tight-binding model parametrized on Density Functional Theory

(DFT) [11]. Authors of Ref. [11] have found that the Young modulus of BNNTs varies between 0.837 and 0.912 TPa for tube diameters ranging from 0.81 to 2.08 nm.

A recent in situ Transmission Electron Microscopy (TEM) bending test has demonstrated that the Young modulus of BNNTs ranges from 0.25 ± 0.04 TPa to 1.11 ± 0.17 TPa [12] for wall thicknesses varying between 0.34 and 0.07 nm, respectively, since the elastic properties depend on the Single-Walled (SW) BNNT thickness considered.

Comparing CNTs with BNNTs, there is an interesting phenomenon: at moderate temperatures CNTs are stronger, while at high temperatures BNNTs become more thermomechanically stable.

As a matter of fact, a combination of their insulating character and the discovered herein remarkable mechanical properties makes SW-BNNTs primarily important for applications in Nanoelectromechanical Systems (NEMS) where electrically insulating and high-strength materials are needed.

Thermal Properties

Several calculations including tight-binding method, DFT, and valence shell model, have been performed in order to investigate the thermal properties of BNNTs [13–15]. The results have shown that BNNTs have a larger low-temperature thermal conductivity [16] than CNTs even when BNNTs have the same phonon mean free path as CNTs. However, it was demonstrated experimentally that pure and collapsed BNNTs are estimated to have thermal conductivity of 18 and $\sim$46 W/mK, respectively [17].

Another remarkable thermal property of BNNTs is their high resistance to oxidation. In air, BNNTs are very stable up to at least 700 °C. Highly crystalline and low-defect BNNTs may be stable up to 900 °C with only the tube caps being oxidized [18]. This more pronounced resistance of BNNTs to oxidation is inherited from the hexagonal BN and also depends on the nanocrystalline structure. This high level of resistance to oxidation allows promising BN nanotube applications at high temperatures.

Although BNNTs are electrically insulating materials, they possess very high thermal conductivity [19]. Thermal conductivity of BNNTs is due to phonons [20]. It has been known that with an increase of the nanotube's diameter, the thermal conductivity can be dramatically decreased. This is because instead of all-layers heat transport in bulky materials, only few shells are involved in thermal transport in nanotubes [21]. Some works have estimated thermal conductivity of individual BNNTs and a range of 120-960 W/mK was found [22].

Magnetic Properties

Theoretically, magnetism of BNNTs was investigated. The O, C, V, Cr, Mn, Ge, F, Be, and H doping were found to induce magnetism in BNNTs [1]. The saturated magnetic moment was predicted to range from 1 to 3.98 μB per doping atom varying from element to element. The main part of magnetic moments comes from the doping atoms other than B and N atoms. The strict restrictions for doping sites make that doping induced magnetism in BNNTs be very difficult to do experimentally.

Optical Properties

The optical band gap of BNNTs is independent of the chirality, this was obtained by a Local-Density Approximation (LDA) calculation [23]. Another interesting feature is the photoelectric effect. A study have demonstrated that unpolarized light can induce a shift current in BNNTs, with a direction along the tube axis [24]. These photoelectric effects can lead to new optoelectronic, optomechanical, and magnetic applications.

With respect to polarizabilities of BNNTs, the polarizability tensors were investigated for several types of SW-BNNTs and compared with corresponding CNTs [25]. The results have shown that BNNTs have smaller magnitudes of the polarizability tensor components than those of CNTs with the same geometry and number of atoms. Polarizability tensor of BNNTs is shown to depend on the tube length, chiralities, light frequency, etc.

1.3 Fabrication techniques

A relevant fact of BNNTs is that they can be made experimentally. The synthesis of BNNTs is far more challenging that the growth of CNTs, and some of the growth techniques used to create CNTs can be used for the growth of BNNTs but some others require very specific growth system and procedures. In this section, some of the BNNTs synthesis methods are described.

Arc-discharge

It is the first technique for the fabrication of both CNTs and BNNTs. BNNTs were firstly fabricated by arc-discharged between a BN-packed tungsten rod and a cooled copper electrode [4]. Arc-discharge ocurred between the tungsten and copper electrodes. The inserted h-BN rod was evaporated indirectly. After the arc-discharge, the gray product was deposited on the copper cathode, which contained some scattered SW-BNNTs. The arc-discharge chamber was cooled by a cold water line.

In the following improved experiments using hafnium diboride (hFB_2) as electrodes, single-wall and double-wall BNNTs were synthesized [26–28]. BNNTs fabricated by arc-discharge possess good crystallization due to a high growth temperature (∼3000 K).

Laser ablation

In this method, the target material was prepared by mixing high-purity h-BN and nanosized Ni and Co powders [29]. The target was then placed inside a long quartz tube heated by a tube furnace. An excimer laser with a wavelength of 248 nm was focused on the target to initiate ablation. At optimum laser pulsed energy and oven temperature (1200 °C), the ablated laser plumes were carried by the flowing gas and collected on the water-cooled copper collector. BNNTs with diameters ranging from 1.5 to 8 nm were obtained together with other amorphous by-products. Comparison of the structure of the BNNTs synthesized with different carrier gases revealed an interesting phenomenon. BNNTs obtained in inert argon and helium gases were dominated with SW-BNNTs. When nitrogen was used as the carrier gas, the BNNTs were dominated with double-wall structures. No BNNTs with more than four walls were observed.

Ball-milling

This method was first developed in 1999 [30]. It consists of using ball-milling of a hexagonal BN powder to generate highly disordered or amorphous nanostructures, followed by annealing at a temperature up to 1300 °C. BNNTs and bamboo-like BN nanostructures were obtained. No specific catalysts were used. Fe species coming from a stainless-steel container were proposed to be effective catalysts for the growth of BNNTs. The yield ratio of pure BNNTs was rather low as the products were mixed with a large amount of amorphous materials. Subsequently, experiments were designed to improve the quality and purity of ball-milled BNNTs by using a boron powder as the precursor, introducing NH_3 as a protection gas during ball-milling and optimizing annealing conditions [31–35]. The characteristics of BNNTs produced by this method were indeed improved. The yield of BNNTs was increased and their diameters were reduced to less than 10 nm. However, the purity of the samples still remained low, because iron particles were produced and mixed with boron powder in the milling process, and the content of iron particles was about 1.5 at.% [34]. By this method, large quantities of BNNTs are produced. This method is a practical production with low cost.

Chemical vapor deposition (CVD)

The initial CVD growth of BNNTs was reported in 2000 [36]. Borazine was used as a precursor and Co, Ni, NiB and Ni_2N particles were found to be effective catalysts. The growth temperature was 1000-1100 °C, which had been common in most CVD growths of BNNTs. Yap and co-workers [37] realized a low temperature (600 °C) growth of BNNTs by a plasma enhanced pulsed-laser deposition. It is surprising that the BNNTs have been claimed to possess good crystallinity. To meet the demands of large-scale synthesis of highly pure BNNTs, a CVD method using boron and metal oxide as the reactants (BOCVD) has been developed [38–40]. This method separates a boron precursor (boron powder plus metal oxide) from the as-grown BNNTs during the growth. This preserves BNNTs from contamination by the precursors and guarantees their ultimate purity. Various metal oxides were found to be effective for the growth of BNNTs. A mixture of MgO and FeO or MgO and SnO was found to be the best [40]. So far, grams level of BNNTs can be fabricated by this method. Also significant efforts were made to realize world-first kilogram level

growth. Another promising CVD method for the mass production of BNNTs has recently been developed utilizing a floating catalyst. This might be further optimized toward the realization of a continuous growth of BNNTs [41].

1.4 Biocompatibility of BNNTs

The properties of BNNTs make them suitable for biomedical applications. However, for a nanomaterial, biocompatibility should be considered prior to any practical applications. Several works have been made to study the toxicity of BNNTs in human cells [42–46]. In this experiments, polyethyleneimine (PEI)-coated BNNTs were used for in vitro test on a human neuroblasma cell line [42, 43]. The results indicated very good cell viability up to a concentration of 5.0 mg/ml of BNNTs in the cell culture medium. At a higher concentration, a moderate toxicity was noticed, which was assigned to PEI coating instead of BNNTs themselves. Chen et al. [47] used pristine BNNTs for in vitro tests although the authors formed aggregates in the culture media. The experimental results have shown that BNNTs do not appear to inhibit cell growth or induce apoptotic pathways in the cells. In contrast, carbon nanotubes (CNTs) have been shown to induce apoptosis in the cells. The surface of functionalized BNNTs may have glycodendrimers capable of interacting with proteins and cells [47]. Moreover, BNNTs could deliver DNA oligomers to the interior of cells with no apparent toxicity. These studies have demonstrated relevant safety of BNNTs, which may have potential applications in the biological systems where the toxicity of CNTs is a problem.

Very recent studies have been carried out to provide new data of the interactions between BNNTs and living systems [48,49]. Ciofani et al. [49] have shown that no significant adverse effects were found up to 7 days since the BNNTs were injected in rabbits at a dose up to 10 mg/kg, and no impairments in blood, liver and kidney functionality were highlighted. Moreover, a terminal half-life circulation of about 90 min was found. All the collected data are very promising, suggesting the optimal biocompatibility of BNNTs, and thus enabling their exploitation in nanomedicine as nanotransducers and nanocarriers.

1.5 Applications of BNNTs

The discussion on applications of BNNTs is rare in the literature due to present limitations and challenges of mass production, i.e., the control of the synthesis and properties of BNNTs. However, there are some works that focus on potential applications of BNNTs, as will be described next.

Hydrogen storage

Hydrogen is regarded as an ideal and nonpolluting energy source that may become an alternative to replace current energy sources. However, hydrogen storage is among the obstacles toward real hydrogen energy technology. The hydrogen storage of BNNTs was intensively studied by theoretical calculations. The ionic character of B-N bonds may induce extra dipole moments favorable for stronger adsorption of hydrogen. However, totally different results were obtained due to different models and calculation methods adopted. Some results have shown that both physisorption and chemisorption are not energetically favored, thus BNNTs are not good candidates for hydrogen storage [50]. Other results stated that hydrogen storage capacity of BNNT arrays is obviously much better than for CNTs, and can reach or even exceed the commercial standard presented by the US Department of Energy [51]. Thus, it is difficult to make a well-established judgment on hydrogen storage capacity of BNNTs using only theory. However, the presence of defects, doping, and/or deformation of BNNTs may remarkably improve their ability to absorb hydrogen. Metal-doped BNNTs might be even better for hydrogen storage [52], because the presence of defects could enhance the adsorption of hydrogen atoms on BNNTs and reduce the dissociation barrier of the hydrogen molecule on their walls. Another investigation claimed that moderate substitutional doping in materials with ionic-like bonding, such as carbon-doped BNNTs, could enhance the binding energies of hydrogen, making them optimal for storage [53].

Experimentally, Ma et al. have shown that multiwalled BNNTs can absorb 1.8-2.6 wt.% hydrogen under ∼10 MPa at room temperature [54]. Chen et al. [55] used an electrochemical measurement to test hydrogen accumulation in BNNTs and a disappointing result of only ∼0.25 wt.% of hydrogen absorption was obtained The experimental studies on hydrogen storage of

BNNTs are still very few, and similar to theoretical works, discrepant results have been reported. There have still no detailed and comprehensive studies in regard of hydrogen storage of BNNTs.

Water desalination

There is an urgent need to make the process of desalination more effective and less costly than the currently available methods, in order to offer a possible solution to the needs of fresh water of the growing population. Nanotube-based water-purification devices have the potential to transform the area of desalination and demineralization through their ability to remove salts and heavy metals without significantly affecting the fast flow of water molecules. BNNTs have shown superior water flow properties compared to CNTs, and are thus expected to provide a more efficient water purification device. Using molecular dynamics simulations it is shown that a (5,5) BNNT embedded in a silicon nitride membrane can, in principle, obtain 100% salt rejection at concentrations as high as 1 M (molar concentration) owing to a high energy barrier while still allowing water molecules to flow at a rate as high as 10.7 water molecules per nanosecond [56]. Furthermore, ions continue to be rejected under the influence of high hydrostatic pressures up to 612 MPa. When the nanotube radius is increased to 4.14 Å the tube becomes cation-selective, and at 5.52 Å the tube becomes anion-selective.

Nanofillers for composite materials

The remarkable properties of BNNTs, such as high elastic modulus and high thermal conductivity make them advantageous for novel nanofillers in composite materials to obtain mechanical reinforcement, high thermal conductivity and a low coefficient of thermal expansion in a matrix. BNNTs composite studies were initiated in recent years because of the difficulties in the high-yield synthesis of pure BNNTs. So far, polymeric, ceramic and metal composites were fabricated.

BNNTs′ polymeric composites can be novel packaging materials. They can be efficient for electronic devices. The high thermal conductivity can help heat-releasing, which allows high performance of a device. Moreover, due to a wide band gap of BNNTs, polymeric composites with low BNNTs′ fraction can keep decent transparency. Thus, they can be used as effective packaging materials for organic photovoltaic devices [57].

The resistance of BNNTs to oxidation is a solid advantage for the fabrication of BNNTs ceramic composites. Bansal et al. [58] firstly used BNNTs to fabricate barium calcium aluminosilicate glass composites. The addition of 4 wt.% BNNTs increases the glass strength up to 90% and the fracture toughness up to 35%. Huang et al. [59] investigated mechanical properties of Al_2O_3-BNNTs and Si_3N_4-BNNTs composites. No obvious Vickers hardness and Young′s modulus improvement were revealed. However, it was observed that BNNT small additions had been able to dramatically enhance a high-temperature superplastic deformation (SPD) of Al_2O_3 and Si_3N_4, which was explained in line with the microstructure variations at grain boundaries and interactions between the BNNTs and a matrix.

Recently, for the first time, Al-BNNT composite ribbons (up to 1 m long) with various multi-walled BNNT contents (0.5 to 3.0 wt.%) were fabricated [60]. The BNNTs are randomly oriented within the Al matrix and partially participate in carrying the tensile load, as evidenced by their presence and breakage at the composite fracture surfaces. The ultimate tensile strength of the composite ribbons with 3 wt.% of BNNT at room temperature was more than doubled (145 MPa) compared to non-loaded pure Al ribbons (60 MPa).

Bio-applications

The nucleic acid bases, being the key components of the genetic macromolecules (DNA and RNA), play a central role in all biological systems and thus have been a focus of intense research activities over the past five decades. Amino acids play central roles both as building blocks of proteins and as intermediates in metabolism. Recently, there has been a great interest in undestanding the interaction between biological molecules and matter, especially nanostructured materials such as CNTs and BNNTs.

Mukhopadhyay et al. [61] investigated the adsorption of the nucleobases (i.e., adenine, guanine, cytosine, thymine, and uracil) on the outer wall of a (5,0) SW-BNNT. The calculations were performed using the plane wave pseudopotential approach within the LDA of DFT. They also calculated the polarizability of a BN sheet which is significantly smaller than that of the graphene at the LDA level of theory, this suggest that the tubular surface of a BNNT can be expected to be less polarizable than that of a CNT. However, the interaction between BNNTs and nucleobases

is dominated by the van der Waals (vdW) forces. The results show that guanine exhibits the strongest binding when physisorbed on BNNT compared to the other nucleobases, and this might be used in sensing and distinguishing this molecule from other base molecules.

BNNTs can be used as biosensors, as demonstrated in 2013 by Zhong et al. [62]. The I-V characteristics of nucleobase-conjugated BNNT sandwiched between gold electrodes are studied using the LDA-DFT method together with the non-equilibrium Green′s function method. The calculated results show a direct relationship between the strength of binding of the molecules adsorbed on BNNTs and their effect on the transport properties of the conjugated system. Guanine leads to a higher current in the conjugated BNNTs due to opening of new conduction channels near the Fermi energy of the bioconjugated system. The results therefore suggest the suitability of BNNTs for biosensing applications.

Taking into account the unique properties of BNNTs and their applications, in this work we investigate the interaction between BNNTs and some biological molecules, among which are three amino acids and five nitrogenous bases: glycine, serine, cysteine, cytosine, thymine, uracil, adenine and guanine. Each molecule is placed inside the BNNT. The calculations are carried out using different approaches like Hartree-Fock, DFT, and the latest version of DFT with dispersion correction (DFT-D3), which is a method that has been proved to be a good choice for problems that require an evaluation of the interactions between molecules and between molecules and less dense material [63].

The outline of this thesis is as follows. In Chapter 2, we describe the theory on which the calculations are based. Also, we present different methods like Hartree-Fock, post Hartree-Fock, Density functional theory, and van der Waals interactions. In Chapter 3, we show our results, including figures of the different systems considered and their binding energies which are important because they describe the adsorption of the different molecules within the BNNT. Also, we make a comparation of the results obtained with the different approximations considered. In Chapter 4, we present our conclusions and future work.

2 Theoretical Framework

The study of the properties of matter at a very small scale is performed according to the laws of quantum mechanics. In general, matter is a set of interacting atoms, sometimes under the influence of an external field. It is possible to write the Hamiltonian of a system in the following general form [64]

$$\begin{aligned}\hat{H} = & - \sum_{I=1}^{P} \frac{\hbar^2}{2M_I}\nabla_I^2 - \sum_{i=1}^{N} \frac{\hbar^2}{2m}\nabla_i^2 + \frac{e^2}{2}\sum_{I=1}^{P}\sum_{J\neq I}^{P} \frac{Z_I Z_J}{|\mathbf{R}_I - \mathbf{R}_J|} \\ & + \frac{e^2}{2}\sum_{i=1}^{N}\sum_{j\neq i}^{N} \frac{1}{|\mathbf{r}_i - \mathbf{r}_j|} - e^2 \sum_{I=1}^{P}\sum_{i=1}^{N} \frac{Z_I}{|\mathbf{R}_I - \mathbf{r}_i|}, \end{aligned} \tag{2.1}$$

where $\mathbf{R} = \{\mathbf{R}_l, \quad l = 1, ..., P\}$ is a set of P nuclear coordinates, and $\mathbf{r} = \{\mathbf{r}_i, \quad i = 1, ..., N\}$ is a set of N electronic coordinates. Z_I y M_I are the nuclear charges and masses, respectively. In Eq. (2.1) the first term represents the kinetic energy of the nuclei, the second term is the kinetic energy of the electrons, the third term represents the nuclei interaction, the fourth term is the interaction between electrons, and the last term is the interaction between electrons and nuclei.

In order to analyze each system it is necessary to solve the Schrödinger equation. However, the only problems that have analytic solution are those related to one particle (free particle) or two particles interacting (hydrogen atom). When there are more than two particles interacting (atoms, molecules, etc.) it becomes necessary to use approximate methods to solve the Schrödinger equation.

A first approach is the adiabatic or Born-Oppenheimer approximation, in which the nuclei are considered to be located in fixed positions because their motion is much slower compared to the motion of electrons, as a result of that the nuclei are thousands of times heavier than electrons [64]. Therefore, the motion of electrons in the fixed nuclear environment is calculated from the Schrödinger equation, and in the Hamiltonian of Eq. (2.1) should be considered only

the terms involving electrons, so Eq. (2.1) is simplified as follows

$$\hat{H} = -\frac{\hbar^2}{2m}\sum_{i=1}^{N}\nabla_i^2 + \frac{e^2}{2}\sum_{i=1}^{N}\sum_{j\neq i}^{N}\frac{1}{|\mathbf{r}_i - \mathbf{r}_j|} - e^2\sum_{I=1}^{P}\sum_{i=1}^{N}\frac{Z_I}{|\mathbf{R}_I - \mathbf{r}_i|}. \tag{2.2}$$

2.1 Variational Method

In 1900 W. Ritz generalized Rayleigh variational principle by proposing a variational method to solve approximately an eigenvalue equation [65]. This method has been successfully applied in quantum mechanics (in theory of atoms and molecules, etc.).

In the case of a time-independent system described by the Hamiltonian $\hat{H}$, the time-independent Schrödinger equation must be solved

$$\hat{H}\psi_k = E_k\psi_k, \tag{2.3}$$

where ψ_k is the eigenfunction corresponding to eigenvalue E_k. The index k is chosen such that the energy increases with it ($E_k > E_{k'}$ for $k > k'$). The ground state is considered with $k = 0$ and its corresponding energy is E_0. An arbitrary normalized function Φ is chosen, which is expressed in terms of the base ψ_k [65]

$$\Phi = \sum_k a_k\psi_k, \tag{2.4}$$

because Φ is normalized, the following holds

$$\sum_k |a_k|^2 = 1. \tag{2.5}$$

The expectation value of $\hat{H}$ calculated with the arbitrary function Φ is

$$\begin{aligned}\langle\Phi|\hat{H}|\Phi\rangle &= \sum_k\sum_{k'} a_k^* a_{k'}\int_\infty^\infty \psi_k^*\hat{H}\psi_{k'}dV \\ &= \sum_k\sum_{k'} a_k^* a_{k'}E_{k'}\delta_{kk'} = \sum_k |a_k|^2 E_k \geq E_0\sum_k |a_k|^2.\end{aligned} \tag{2.6}$$

Using Eq. (2.5) yields

$$\langle\Phi|\hat{H}|\Phi\rangle \geq E_0. \tag{2.7}$$

Therefore, the expectation value of a Hamiltonian calculated with an arbitrary normalized function is greater than or, at best, equal to the ground state energy of the Hamiltonian itself, i.e.,

the eigenfunction corresponding to the ground state is the normalized function that minimizes the expectation value of the Hamiltonian. The quality of the result depends on the quality of the trial function Φ. In general, mathematically simple functions are chosen. For example, in the case of the ground state should not have nodes, Φ must decrease exponentially at infinity (for bound states), must be respected the symmetries of the problem, etc. By making an appropriate choice of the trial function, one or two parameters are enough to obtain reasonable approximations.

For excited states, the trial function must be orthogonal to the lower states. If solutions are known up to $n-1$ state, then for the state n

$$\Phi_n = \sum_{k \geq n} a_k \psi_k. \tag{2.8}$$

Due to the orthogonality condition

$$\langle \psi_l |\, \Phi_n \rangle = 0, \tag{2.9}$$

for $l = 0, 1, ..., n-1$. Therefore, the expectation value of a Hamiltonian calculated with an arbitrary function for the state n is

$$\langle \Phi_n \,|\, \hat{H} \,|\, \Phi_n \rangle = \sum_{k \geq n} |a_k|^2 E_k \geq E_n. \tag{2.10}$$

If the approximate functions of the wave functions for $k \leq n-1$ are known, then the accumulated errors make this method be used successfully to obtain only the first excited states.

Equation (2.7) shows that the spatial distribution of particles corresponds to the one that minimizes the average energy of the system. If the ground state function ψ is known, then the expectation value of the Hamiltonian with this function, which corresponds to the energy, is

$$E = \langle \psi \,|\, \hat{H} \,|\, \psi \rangle, \quad with \quad \langle \psi |\, \psi \rangle = 1. \tag{2.11}$$

Considering an arbitrary function Φ

$$\begin{aligned} |\Phi\rangle &= |\psi\rangle + |\delta\psi\rangle, \\ \langle\Phi| &= \langle\psi| + \langle\delta\psi| \end{aligned} \tag{2.12}$$

with $|\delta\psi\rangle$ and $\langle\delta\psi|$ arbitrary but keeping the normalization. Substituting Eq. (2.12) in $\langle \Phi \,|\, \hat{H} \,|\, \Phi \rangle$ it follows that the energy change at first order is

$$\delta E = \langle \psi \,|\, \hat{H} \,|\, \delta\psi \rangle + \langle \delta\psi \,|\, \hat{H} \,|\, \psi \rangle, \tag{2.13}$$

with $\langle \delta\psi |\, \psi\rangle + \langle \psi |\, \delta\psi\rangle = 0$ in order to conserve the normalization. To minimize δE the normalization condition is taken into account by the Lagrange's method of undetermined coefficients,

$$\langle \psi \,|\, \hat{H} \,|\, \delta\psi \rangle + \langle \delta\psi \,|\, \hat{H} \,|\, \psi \rangle - \lambda[\langle \delta\psi |\, \psi\rangle + \langle \psi |\, \delta\psi\rangle] = 0. \tag{2.14}$$

Equation (2.14) can be rewritten as

$$\langle \psi \,|\, \hat{H} - \lambda \,|\, \delta\psi \rangle + \langle \delta\psi \,|\, \hat{H} - \lambda \,|\, \psi \rangle = 0. \tag{2.15}$$

The previous condition must hold for any pair $|\delta\psi\rangle$, $\langle\delta\psi|$ and it is fulfilled if the Schrödinger equation and its adjoint are satisfied,

$$\hat{H}\,|\psi\rangle = \lambda\,|\psi\rangle\,, \quad \langle\psi|\,\hat{H} = \lambda\,\langle\psi|\,, \quad \lambda = \langle\hat{H}\rangle = E. \tag{2.16}$$

By choosing $|\delta\psi\rangle = \epsilon(\hat{H} - \lambda)\,|\psi\rangle$, with ϵ infinitesimal and real, and substituting it in Eq. (2.15) yields

$$2\epsilon\,\langle \psi \,|\, (\hat{H} - \lambda)(\hat{H} - \lambda) \,|\, \psi \rangle = 0. \tag{2.17}$$

The fact that $|\psi\rangle$ is solution of the Schrödinger equation ensures that the average energy in each discrete level has an extreme value versus small arbitrary changes of the corresponding stationary distribution, and this extreme value is a minimum. By minimizing the energy, the parameters of the trial function that minimizes the energy are obtained.

The variational method has been successfully applied to the solution of important problems. When the number of parameters used is small and the problem is simple, analytical methods can be used to obtain a solution. When the number of parameters is large, then numerical methods are used.

Time-dependent variational principle

It is possible to obtain a variational formulation limited from the Frenkel variational principle, when is used a trial wave function similar to the following [66]

$$\Psi(\mathbf{r},t) = \phi(\mathbf{r},t)\,\langle\phi|\,\phi\rangle^{-1/2}\,exp\left[(i\hbar)^{-1}\left(E_0^{(0)}t + \int_{-\infty}^{t} Re\Delta E(t')dt'\right)\right], \tag{2.18}$$

where

$$\Delta E(t) = \left\langle \phi_0^{(0)} \left| H^{(1)} \right| \phi \right\rangle, \tag{2.19}$$

$H^{(1)}$ is the perturbation Hamiltonian.

The time-dependent variational principle given by Frenkel is [66]

$$\left\langle \delta\tilde{\Psi} \right| H_0 + H^{(1)} - i\hbar(\partial/\partial t) \left| \tilde{\Psi} \right\rangle = 0, \tag{2.20}$$

where $\tilde{\Psi}(\mathbf{r}, t)$ is an approximate solution of the time-dependent Schrödinger equation

$$\left[H_0(\mathbf{r}) + H^{(1)}(\mathbf{r}, t) - i\hbar(\partial/\partial t) \right] \Psi(\mathbf{r}, t) = 0, \tag{2.21}$$

and $\delta\tilde{\Psi}(\mathbf{r}, t)$ is an arbitrary variation about $\tilde{\Psi}(\mathbf{r}, t)$.

The validity of the Frenkel principle is not restricted to the perturbation case of interest but applies to an arbitrary time-dependent Hermitian Hamiltonian. Equation (2.20) is not in the form of the variation of a functional set equal to zero. Consequently, unlike the Ritz variation principle, which can provide a bound to the total energy in the static case, the Frenkel variational principle of Eq. (2.20) appears not to furnish a bound to a property of physical interest. What is highly desirable is a variational procedure which does provides such a bond, especially on the response of a system to an external perturbation.

To study the possibility of obtaining a bound from the Frenkel principle, Eq. (2.20) adds to its complex conjugate and is obtained

$$\delta \left\langle \tilde{\Psi} \right| H_0 + H^{(1)} - i\hbar(\partial/\partial t) \left| \tilde{\Psi} \right\rangle + i\hbar(\partial/\partial t) \left\langle \tilde{\Psi} \right| \delta\tilde{\Psi} \Big\rangle = 0. \tag{2.22}$$

This form of the Frenkel principle is perfectly general and provides the correct solution of the Schrödinger equation if a sufficiently flexible trial function is employed.

The Frenkel variational principle in the form of Eq. (2.22) does not require an explicit normalization constraint. That is, although the variation $\delta\tilde{\Psi}(\mathbf{r}, t)$ in Eq. (2.22) can be carried out subject to a normalization constraint ($\langle \Psi | \Psi \rangle = 1$), the Lagrange multiplier introduced to satisfy this demand can be set equal to zero, since the Hermiticity of the Hamiltonian and the resulting time-dependent Schrödinger equation itself will insure that the correct solution has a constant norm.

2.2 Hartree-Fock (Self-Consistent Field, SCF) method

An approximate method to solve the Schrödinger equation for systems involving more than one electron and for complex atomic, molecular and nuclear problems is the Self-Consistent Field (SCF) method, proposed by D. R. Hartree in 1928 and derived using the variational method by V. A. Fock in 1930 [65]. Considering the atomic case as example, the basic idea of the Hartree-Fock method is to consider that each electron moves in an average field produced by the rest of the electrons and the nucleus and that, in turn, contributes to the effective field for the rest of electrons. Given the complexity of the calculation, it is used only in numerical form.

Considering an atom containing N electrons and neglecting the spin-orbit coupling. The Hamiltonian of the atom is [65]

$$\hat{H} = \sum_k \hat{H}_0(\mathbf{r}_k) + \sum_{k<l} V(\mathbf{r}_k, \mathbf{r}_l) = \sum_k \hat{H}_0(\mathbf{r}_k) + \frac{1}{2}\sum_{l\neq k} V(\mathbf{r}_k, \mathbf{r}_l), \tag{2.23}$$

where $\hat{H}_0(\mathbf{r}_k)$ corresponds to the Hamiltonian of the kth independent electron, and $V(\mathbf{r}_k, \mathbf{r}_l)$ corresponds to the interaction between electrons. The previous terms can be expressed, respectively, as follows

$$\hat{H}_0(\mathbf{r}_k) = -\frac{\hbar^2}{2m_k}\nabla_k^2 - \frac{Ze^2}{\mathbf{r}_k}, \tag{2.24}$$

$$V(\mathbf{r}_k, \mathbf{r}_l) = \frac{e^2}{|\mathbf{r}_k - \mathbf{r}_l|}. \tag{2.25}$$

It is proposed that the trial function is a product of wave functions of independent particles

$$\psi(\mathbf{r}_1, \mathbf{r}_2, ..., \mathbf{r}_N) = \varphi_1(\mathbf{r}_1)\varphi_2(\mathbf{r}_2)\cdots\varphi_N(\mathbf{r}_N). \tag{2.26}$$

The expectation value of the Hamiltonian calculated with the trial function ψ is

$$\langle\hat{H}\rangle = \sum_k \int \varphi_k^* \hat{H}_0 \varphi_k d^3r_k + \frac{1}{2}\sum_{l\neq k}\int \varphi_k^*\varphi_l^* V(\mathbf{r}_k, \mathbf{r}_l)\varphi_k\varphi_l d^3r_k d^3r_l. \tag{2.27}$$

It is desired that $\langle\hat{H}\rangle$ be a minimum versus small arbitrary changes of the trial function. By varying φ_k^* leaving φ_k fixed, is obtained

$$\delta\langle\hat{H}\rangle = \sum_k \int \delta\varphi_k^* \left[\hat{H}_0 + \sum_{l\neq k}\langle l\,|\,V(k,l)\,|\,l\rangle\right]\varphi_k d^3r_k, \tag{2.28}$$

$\delta\langle\hat{H}\rangle$ must vanish. However, the $\delta\varphi_k^*$ are not independent, from the normalization constraint of each wave function is obtained

$$\int \delta\varphi_k^* \varphi_k d^3 r_k = 0. \tag{2.29}$$

In order to take into account the constraints when calculating $\delta\langle\hat{H}\rangle$ the Lagrange method of undetermined multipliers is used. Multiplying Eq. (2.29) by the undetermined constant E_k, and then is substracted from Eq. (2.28), obtaining

$$\sum_k \int \delta\varphi_k^* \left[\hat{H}_0 + V_k - E_k\right] \varphi_k d^3 r_k = 0, \tag{2.30}$$

where

$$V_k = \sum_{l\neq k} \langle l \,|\, V(k,l) \,|\, l \rangle = \sum_{l\neq k} \int \varphi_l^* V(\mathbf{r}_k, \mathbf{r}_l) \varphi_l d^3 r_l. \tag{2.31}$$

V_k represents the Hartree potential or effective potential, and refers to the average potential at point $\mathbf{r}_k$ occupied by the electron k, produced by the rest of electrons. To satisfy Eq. (2.30), the term $\left[\hat{H}_0 + V_k - E_k\right] \varphi_k$ must vanish, and this yields to the following system of Hartree equations

$$\left(\hat{H}_0 + V_k\right) \varphi_k = E_k \varphi_k. \tag{2.32}$$

Each Hartree equation is the Schrödinger equation for an electron that moves in the field produced by the nucleus (interaction contained in $\hat{H}_0$) and the average potential V_k produced by the rest of electrons. This procedure has allowed to convert a problem of N coupled particles into N problems of single particle, where each one moves in a common potential determined by the rest.

The Hartree approximation treats electrons as distinguishable particles (classical). However, electrons are indistinguishable particles with fractional spin (1/2), i.e., fermions, and the Pauli exclusion principle states that two fermions can not occupy the same quantum state because the wave function must be antisymmetric in the exchange of particles. This means that if two electrons are exchanged, then the wave function must change sign. The Hartree approximation does not include this feature, i.e., the Pauli exclusion principle has not been taken into account in the solution of the problem. This was corrected by Fock by proposing a linear combination of Hartree functions, taking into account the spinorial dependence. This antisymmetric function can be expressed as a Slater determinant

$$\Psi(\xi_1, \xi_2, ..., \xi_N) = \sum_{P_k} \hat{P}_k a_{P_k} \varphi_1(\xi_1)\varphi_2(\xi_2)\cdots\varphi_N(\xi_N), \tag{2.33}$$

where $\xi_i = (\mathbf{r}_i, \sigma_i)$ is the set of spatial and spinorial variables of the particle i, $\hat{P}_k$ is the exchange operator, and a_{P_k} are phase factors, particularly the wave functions that are in turn simultaneous eigenfunctions of the complete set of operators $\hat{P}_{ij}$ correspond to $a_{P_k} = 1$ for the symmetric case, and $a_{P_k} = (-1)^{r_{P_k}}$ for the antisymmetric case, where r_{P_k} is the number of pairs of particles that must be exchanged to achieve the permutation P_k. In Eq. (2.33) the sum runs over all the possible permutations P_k of the pairs of identical particles.

In the absence of spin-orbit coupling, a system of equations analogous to Hartree but more complex is obtained, which constitutes the Hartree-Fock equations

$$\left(\hat{H}_0 + V_k\right)\varphi_k - \sum_{l\neq k} V_{kl}\varphi_l = E_k\varphi_k, \tag{2.34}$$

where

$$V_{kl} = \int \varphi_k^* V(k,l)\varphi_l d^3 r_l = \langle k\,|\,V(k,l)\,|\,l\rangle\,. \tag{2.35}$$

V_{kl} is the exchange potential, which considers the exchange of electrons between different orbitals. The Pauli exclusion principle is considered implicit, because each electron can only be in a different orbital. Hartree equations are obtained from Hartree-Fock equations if the exchange effects are neglected.

The numerical procedure to solve them consists of finding a self-consistent solution as follows [65]: an initial selection $\varphi_k^{(0)}$ of functions φ_k is made, with which is calculated a first approximation to the potentials V_k and V_{kl}, these potentials are introduced into the system of equations that must be solved to determine a new approximation $\varphi_k^{(1)}$ of the wave functions. The potentials are recalculated and the process is repeated until the wave functions obtained match those of the previous step, i.e., until convergence is achieved. This is an iterative method.

Once the solutions have been determined, the energy is calculated with them by

$$E = \sum_k E_k - \frac{1}{2}\sum_k\sum_{l\neq k}\left[\langle kl\,|\,\hat{V}(k,l)\,|\,kl\rangle - \langle kl\,|\,\hat{V}(k,l)\,|\,lk\rangle\right]. \tag{2.36}$$

The E_k represent an approximation to the ionization energy associated with each electron.

The Hartree-Fock approximation can be used to estimate the electronic structure of molecular systems. It also provides a good description of the interatomic bond. However, this method has

the limitation that the wave function of a many-body system is not well represented by a single Slater determinant. Another antisymmetric wave functions exist that can not be written in this way and, therefore, are not accessible within the Hartree-Fock approximation [64].

Restricted Hartree-Fock method

The wave function Ψ can be approximated to a function of the form of a Slater determinant (Eq. (2.33)), which is an antisymmetrized product of N orthonormal spin-orbitals $\varphi_i(\mathbf{r})$, each one is in turn a product of a spatial orbital $\phi_k(\mathbf{r})$ and a spin function $s(\sigma) = \alpha(\sigma)$ or $\beta(\sigma)$ [69]. Equation (2.33) can be rewritten as

$$\Psi(\xi_1, \xi_2, ..., \xi_N) = \frac{1}{\sqrt{N!}} det[\varphi_1(\xi_1)\varphi_2(\xi_2)\cdots\varphi_N(\xi_N)], \tag{2.37}$$

where N is the number of electrons.

The restricted Hartree-Fock method (RHF) is used in closed-shell systems having an even number of electrons. It is customary to suppose, in this case, that the spatial components of the spin-orbitals are identical for each member of a pair of electrons. The N orbitals φ_i are taken to comprise $N/2$ orbitals of the form $\phi_k(\mathbf{r})\alpha(s)$ and $N/2$ orbitals of form $\phi_k(\mathbf{r})\beta(s)$. Therefore, the Hartree-Fock wave function is [69, 70]

$$\Psi = \frac{1}{\sqrt{N!}} \begin{vmatrix} \varphi_1^\alpha(\xi_1) & \varphi_1^\beta(\xi_1) & \cdots & \varphi_{N/2}^\beta(\xi_1) \\ \varphi_1^\alpha(\xi_2) & \varphi_1^\beta(\xi_2) & \cdots & \varphi_{N/2}^\beta(\xi_2) \\ \vdots & \vdots & \ddots & \vdots \\ \varphi_1^\alpha(\xi_N) & \varphi_1^\beta(\xi_N) & \cdots & \varphi_{N/2}^\beta(\xi_N) \end{vmatrix}, \tag{2.38}$$

where $\varphi_i^\alpha(\xi_j) = \phi_i(\mathbf{r}_j)\alpha(\sigma_j)$ y $\varphi_i^\beta(\xi_j) = \phi_i(\mathbf{r}_j)\beta(\sigma_j)$. This equation is known as restricted Hartree-Fock wave function.

In the case of open-shell systems there are two procedures: restricted and unrestricted. In the restricted open-shell formalism, all electrons except those occupying open-shell orbitals are forced to occupy doubly occupied spatial orbitals. For example, the restricted open-shell wave function for lithium would be of the form

$$\Psi = \frac{1}{\sqrt{6}} det|\varphi_{1s}^\alpha(\xi_1)\varphi_{1s}^\beta(\xi_2)\varphi_{2s}^\alpha(\xi_3)|, \tag{2.39}$$

in which the first two spin-orbitals in the Slater determinant (1s spin-orbitals) have the same spatial wave function. However, the restricted open-shell formalism imposes a severe constraint on the wave function; while the $1s\alpha$ electron has an exchange interaction with the $2s\alpha$ electron, the $1s\beta$ electron does not and, as a result, the variational ground-state energy is usually not accurate.

The unrestricted open-shell formalism will be described next.

Unrestricted Hartree-Fock method

When the number of electrons is not even, the unrestricted open-shell Hartree-Fock method (UHF) is used. In this case, spatial parts of spin-orbitals with α spin are allowed to be different from spatial parts of spin-orbitals with β spin, even within a single pair of electrons [69]. Furthermore, orthogonality between all α-spin spin-orbitals and all β-spin spin-orbitals is still preserved. For instance, the UHF wave function for lithium would be of the form

$$\Psi = \frac{1}{\sqrt{6}} det|\varphi_a^\alpha(\xi_1)\varphi_b^\beta(\xi_2)\varphi_c^\alpha(\xi_3)|, \tag{2.40}$$

in this function all three spatial orbitals are different. By relaxing the constraint of occupying orbitals in pairs, the unrestricted open-shell formalism gives a lower variational energy than that of the restricted open-shell formalism. However, a disadvantage of the UHF approximation is that the total spin angular momentum is not well defined for a UHF wave function.

The UHF method can also be used for an even number of electrons. Often, the UHF method gives no energy lowering over the RHF method, but there are important cases in which energy lowering is found. For example, the UHF description of bond breaking in H_2 gives the proper dissociation products, while the RHF description of H_2 gives unrealistic ones [69].

The UHF wave function is often used as a first approximation to the true wave function, even if the discrepancy is significant.

Coupled Hartree-Fock method

The coupled Hartree-Fock method provides more accurate results, compared with the uncoupled Hartree-Fock method. The coupled method entails a first-order self-consistency requirement, as in the case of Hartree-Fock approximation to the unperturbed wave function.

The coupled Hartree-Fock equations are derived from the Frenkel principle Eq. (2.22), by using a trial function in the form of the Slater determinant

$$\tilde{\Psi}_{HF}(\mathbf{r},t) = (N!)^{-1/2} \left|\tilde{u}_1(\mathbf{r}_1,t)\tilde{u}_2(\mathbf{r}_2,t)\cdots\tilde{u}_N(\mathbf{r}_N,t)\right| \tag{2.41}$$

containing N trial spin-orbitals $\tilde{u}_i(\mathbf{r}_i,t)$, which satisfy the orthonormality requirement

$$\langle \tilde{u}_i |\, \tilde{u}_j \rangle = \delta_{ij}, \quad i,j = 1,2,\ldots,N. \tag{2.42}$$

Substituting Eq. (2.41) into Eq. (2.22), written for an N-electron atom in the Coulomb approximation, with the perturbation Hamiltonian given by the sum of one-electron operators [66]

$$H^{(1)}(\mathbf{r},t) = \sum_{i=1}^{N} g^{(1)}(\mathbf{r}_i,t), \tag{2.43}$$

yields the following

$$\begin{aligned}\delta \left\langle \tilde{\Psi}_{HF} \right| H^{(0)} + H^{(1)} - i\hbar(\partial/\partial t) \left| \tilde{\Psi}_{HF} \right\rangle + i\hbar(\partial/\partial t) \left\langle \Psi_{HF} \right| \delta\tilde{\Psi}_{HF} \Big\rangle = \\ \sum_{i=1}^{N} \Big(\langle\, \delta\tilde{u}_i \,|\, h + g^{(1)} - i\hbar(\partial/\partial t) \,|\, \tilde{u}_i \,\rangle + \textit{complex conjugate} \Big)\,.\end{aligned} \tag{2.44}$$

In Eq. (2.44), $h(\mathbf{r}_i,t)$ is the Fock operator

$$h(\mathbf{r}_i,t) = -(\hbar^2/2m)\nabla_i^2 - (Ze^2/r_i) + v(\mathbf{r}_i,t), \tag{2.45}$$

with the nonlocal Fock potential

$$v(\mathbf{r}_i,t) = \sum_{j=1}^{N} \langle\, \tilde{u}_j \,|\, (e^2/r_{ij})(1 - P_{ij}) \,|\, \tilde{u}_j \,\rangle\,, \tag{2.46}$$

where P_{ij} is the permutation operator for the coordinates of electrons i and j, and $g^{(1)}(\mathbf{r}_i,t)$ is the one-electron perturbation operator. In order to ensure that the variations $\delta\tilde{u}_i(\mathbf{r}_i,t)$ in Eq.

(2.44) are consistent with the orthonormality constraints, the method of Lagrange multipliers, $\lambda_{ij}(t)$, is used. These multipliers are chosen to satisfy Eqs. (2.42). Setting the right hand side of Eq. (2.44) equal to zero and incorporating the orthonormality requirements, is obtained

$$[h(\mathbf{r}_i,t)+g^{(1)}(\mathbf{r}_i,t)-i\hbar(\partial/\partial t)]\tilde{u}_i(\mathbf{r},t)+\sum_{j=1}^{N}\lambda_{ij}(t)\tilde{u}_j(\mathbf{r}_i,t)=0. \tag{2.47}$$

These are the general time-dependent Hartree-Fock equations for the spin-orbitals $\tilde{u}_i(\mathbf{r}_i,t)$.

Various choices for the Lagrange multipliers $\lambda_{ij}(t)$, which insure that Eqs. (2.42) are satisfied can be made. The particularly simple choice is

$$\lambda_{ij}(t)\equiv 0 \quad i,j=1,2,\ldots,N \tag{2.48}$$

which results in the canonical time-dependent Hartree-Fock equations

$$[h(\mathbf{r}_i,t)+g^{(1)}(\mathbf{r}_i,t)-i\hbar(\partial/\partial t)]\tilde{u}_i(\mathbf{r}_i,t)=0. \tag{2.49}$$

That the choice of Eq. (2.48) satisfies Eqs. (2.42) at the solution point comes from Eq. (2.49) and the Hermitian nature of the Fock operator and the perturbation Hamiltonian. From Eq. (2.49) is obtained

$$(\partial/\partial t)\left\langle u_j\right|\left.u_i\right\rangle=0, \tag{2.50}$$

and, consequently, Eqs. (2.42) are satisfied at all times if they are satisfied initially ($t\rightarrow-\infty$).

Equations (2.49) are similar to the complete time-dependent Schrödinger equation, Eq. (2.21), aside from the self-consistency requirement implied by the form of the Hermitian operator of Eqs. (2.45) and (2.46). Applying the time-dependent perturbation theory it is possible to find the solutions $u_i(\mathbf{r}_i,t)$ of Eq. (2.49) [66]

$$u_i(\mathbf{r}_i,t)=\phi_i(\mathbf{r}_i,t)\left\langle\phi_i\right|\left.\phi_i\right\rangle^{-1/2}exp\left((i\hbar)^{-1}\int_{-\infty}^{t}Re\;\epsilon_i(t')dt'\right), \tag{2.51}$$

where $\epsilon_i(t)$ is the Hartree-Fock orbital energy

$$\epsilon_i(t)=\left\langle\phi_i^{(0)}\right|\left.h+g^{(1)}\right|\left.\phi_i\right\rangle\equiv\epsilon_i^{(0)}+\Delta\epsilon_i(t), \tag{2.52}$$

$$\left\langle\phi_i^{(0)}\right|\left.\phi_i\right\rangle=1, \tag{2.53}$$

and the regular part of the spin-orbital, $\phi_i(\mathbf{r}_i, t)$, satisfies

$$[h(\mathbf{r}_i, t) - \epsilon_i^{(0)} - i\hbar(\partial/\partial t)]\phi_i(\mathbf{r}_i, t) + [g^{(1)}(\mathbf{r}_i, t) - \Delta\epsilon_i(t)]\phi_i(\mathbf{r}_i, t) = 0. \tag{2.54}$$

Substituting the perturbation expansions

$$\phi_i(\mathbf{r}_i, t) = \sum_{n=0}^{\infty} \phi_i^{(n)}(\mathbf{r}_i, t), \tag{2.55}$$

$$\Delta\epsilon_i(t) = \sum_{n=1}^{\infty} \epsilon_i^{(n)}(t), \tag{2.56}$$

into Eq. (2.54) gives, to first order [66]

$$[h^{(0)}(\mathbf{r}_i) - \epsilon_i^{(0)}]\phi_i^{(0)}(\mathbf{r}_i) = 0 \tag{2.57}$$

$$[h^{(0)}(\mathbf{r}_i) - \epsilon_i^{(0)} - i\hbar(\partial/\partial t)]\phi_i^{(1)}(\mathbf{r}_i, t) + [g^{(1)}(\mathbf{r}_i, t) + v^{(1)}(\mathbf{r}_i, t) - \epsilon_i^{(1)}(t)]\phi_i^{(0)}(\mathbf{r}_i) = 0, \tag{2.58}$$

where

$$h^{(0)}(\mathbf{r}_i) = -(\hbar^2/2m)\nabla_i^2 - (Ze^2/r_i) + \sum_{j=1}^{N} \left\langle \phi_j^{(0)} \right| (e^2/r_{ij})(1 - P_{ij}) \left| \phi_j^{(0)} \right\rangle \tag{2.59}$$

$$v^{(1)}(\mathbf{r}_i, t) = \sum_{j=1}^{N} \left(\left\langle \phi_j^{(1)} \right| (e^2/r_{ij})(1 - P_{ij}) \left| \phi_j^{(0)} \right\rangle + \left\langle \phi_j^{(0)} \right| (e^2/r_{ij})(1 - P_{ij}) \left| \phi_j^{(1)} \right\rangle \right), \tag{2.60}$$

and

$$\epsilon_i^{(1)}(t) = \left\langle \phi_i^{(0)} \right| v^{(1)} + g^{(1)} \left| \phi_i^{(0)} \right\rangle. \tag{2.61}$$

Equation (2.57) is the unperturbed Hartree-Fock equation in canonical form, and Eq. (2.58) is the first order, time-dependent coupled Hartree-Fock equation. There are coupling terms between first-order orbitals in Eq. (2.58) due to the presence of $v^{(1)}(\mathbf{r}_i, t)$. This introduces the necessity of a first-order self-consistent solution and results in the designation of this approximation as the *coupled* Hartree-Fock approximation. By contrast, the first-order equations in the uncoupled Hartree-Fock approximation do not imply a self-consistent solution. The higher-order coupled Hartree-Fock equations are obtained by including additional terms in the expansion of Eq. (2.54).

2.3 Post-Hartree-Fock methods

The Hartree-Fock wave function represents most of the total energy. The difference $E_{tot} - E_{HF}$ is called, in the context of Hartree-Fock-based methods, the correlation energy [64].

Since the Hartree-Fock wave function is the best single-determinant that can be obtained, then any approach aiming at introducing correlation has to relax this approximation by considering either more than one Slater determinant or antisymmetric wave functions of another type. In principle, any antisymmetric wave function can be written as a linear combination of an infinite number of Slater determinants, although this is not practical. A better option is to include a small number of determinants that produce a large impact at the energetic level. It is important to realize that the picture of individual electrons represented by one-electron wave functions in the mean field of the other electrons does not hold anymore. In general, the correlated many-body wave function cannot be written as an antisymmetrized product of one-electron orbitals. Since the Hartree-Fock wave function is by far the most important contribution to the total energy, the Hartree-Fock wave function is likely to be a good starting point for more complicated calculations.

Considering a general multi-determinant wave function for an N-electron system in the form of a linear combination of a finite number ND (see the explanation of ND in the following lines) of Slater determinants

$$\Psi(\xi_1, \xi_2, ..., \xi_N) = C_0\Psi_0(\xi_1, \xi_2, ..., \xi_N) + \sum_{i=1}^{ND} C_i\Psi_i(\xi_1, \xi_2, ..., \xi_N), \tag{2.62}$$

where $\Psi_0 = \Psi_{HF}$ is the Hartree-Fock solution for the electronic ground state. This ground state wave function corresponds to the N electrons occupying the energetically lowest N spin-orbitals, $[\varphi_i(\mathbf{r}), i = 1, ..., N]$, which for closed-shell systems are the $N/2$ lowest spatial orbitals, each one occupied by a spin up and a spin down electron. Ψ_i are other determinants corresponding to excited states. The larger ND is, the better correlation is represented.

The customary procedure to construct these aditional determinants is to expand the determinantal space by generating determinants that involve unoccupied one-electron states. This means to consider determinants in which an electron has been promoted, e.g., from the highest occupied state in the Hartree-Fock wave function to the first unoccupied state. This type of determinant usually receives the name of single-excitation, or simply single, and is denoted by the letter S. In the same way, determinants in which two electrons have been promoted from occupied to empty one-electron orbitals are called double excitations or doubles, and are indicated with the letter D, and so on. There are different types of excited configurations: those where the total spin of the configuration is the same as in the Hartree-Fock wave function, and those where the total

spin is not conserved.

The number of determinants that can be generated in this way is too large. If the Hartree-Fock equations are solved by expanding the one-electron wave functions in a set of M basis functions, which could be atomic or molecular orbitals. Then the total number of determinants is given by all the possible ways of acommodating N electrons in M orbitals. The number of singles is of order M, the number of doubles is of order M^2, and so on.

Configuration interaction

The simplest multi-determinantal method consists of including in the expansion (2.62) the Slater determinants constructed with the occupied and unoccupied one-electron orbitals of the Hartree-Fock Hamiltonian. With these states left untouched, the expansion coefficients $\{C_i\}$ are optimized in order to minimize the total energy. This method receives the name of *Configuration Interaction* (CI), which results from the fact that correlation is retrieved from contributions to the energy arising from Hamiltonian matrix elements between different Slater determinants, i.e., different electronic configurations. It is possible to express the CI wave function in terms of singles, doubles, triples, etc. [64],

$$\Psi_{CI} = C_0\Psi_{HF} + \sum_{i_S} C_i^S\Psi_i^S + \sum_{i_D} C_i^D\Psi_i^D + \sum_{i_T} C_i^T\Psi_i^T + \cdots , \tag{2.63}$$

Like for Hartree-Fock, it it possible to calculate the expectation value of the total energy of the system

$$E_{CI} = \int\cdots\int \Psi_{CI}^*(\xi_1,\xi_2,...,\xi_N)\hat{H}\Psi_{CI}(\xi_1,\xi_2,...,\xi_N)d\xi_1...d\xi_N \tag{2.64}$$

where the Hamiltonian $\hat{H}$ is given by Eq. (2.23).

It is necessary to find the coefficients $\{C_i\}$ that make the energy E_{CI} minimal. This minimization has to be carried out under the constraint of normalization of the CI wave function. The CI equations are obtained from the constrained minimization condition, in the form of an eigenvalue equation,

$$\mathbf{HC} = E\mathbf{C} \tag{2.65}$$

where $\mathbf{H}$ is the Hamiltonian matrix expressed in the basis of Hartree-Fock determinants. The

lowest eigenvalue corresponds to the ground state energy while higher values correspond to excited states. In the limit of an infinite number of determinants, the CI excited states are the true many-body excitations.

The CI matrix elements can be calculated as in Hartree-Fock, using only one-electron orbitals. A great advantage is that the structure of the Hamiltonian is such that many of these matrix elements are zero.

The method in which all the available determinants are included in the calculation receives the name of *full CI*. It is the most accurate single-reference CI method, being limited only by the size of the basis set. Since this calculation has a very high computational cost, is reserved only for very small systems and used as a benchmark for approximate schemes. The most common CI approximate methods are those in which the expansion is truncated at various levels of excitations. Thus there is the CISD method that truncates the expansion at the level of doubles, or CISDT, which includes also triples. Normally the highest level of truncated CI is that including quadruples (CISDTQ), which appears to be already quite close to full CI. However, CISDTQ is very expensive, because the scaling is M^{10}, which includes the cost of calculating the four-center integrals in a basis set of size M (order M^4), and the number of quadruples, which is of the order M^6. On the other hand, CISD scales as M^6.

Multi-configurational methods

The determinants of the CI expansion are constructed with the fixed Hartree-Fock one-electron eigenstates, this limitation can be relaxed by allowing the determinants to be variationally optimized, together with the expansion coefficients. This method received the name of *multi-configuration self-consistent field* (MCSCF) [64]. The advantage over standard CI methods is not much. Basically, this procedure allows for the one-electron orbitals to be fractionally occupied instead of forcing double occupancy. This is important in the case of systems exhibiting two or more energetically close electronic configurations (sometimes called resonant) with different orbital occupancy, although with the same total spin.

Including a reasonable number of configurations in the optimization procedure is a feasible

task, but the main problem is how to choose these configurations. This has to be done by careful inspection of the problem under consideration, as no general rules exist in this respect. A robust approach in this regard is the *complete active space self-consistent field* method (CASSCF). The configurations are selected by dividing the one-electron orbitals into *active* and *inactive* spaces. Orbitals in the active space, which usually consists of a fraction of highest-lying occupied states, are used to construct all possible configurations by allowing excitations to a few low-lying unoccupied orbitals. The determinants corresponding to these configurations are then optimized, toghether with the expansion coefficients, which can be interpreted as the occupations of the different configurations. The CASSCF method can be considered as a full CI calculation in a restricted configurational space.

For a CI calculation, a multi-configuration wave function with optimized orbitals and occupancies can be used as a reference. In this case, the electronic excitations of all the determinants have to be included, thus increasing the computational cost of the calculation by a factor equal to the number of configurations. Such methods are called *multi-reference configuration interaction* (MRCI), and are usually carried out in the form of truncated CI expansions, e.g. MRCISD.

Perturbative methods

When the exact solution of a particular problem is extremely difficult to obtain or computationally demanding, a usual strategy is to reduce it to a closely related one, for which the exact solution is known. Then, the difference between these two, which is assumed to be small, is treated as a perturbation of the exactly solvable problem (see section 2.4).

One of the central problems in theoretical physics is that of many interacting quantum particles, and it has been faced from different angles. One approximation [67] begins by solving exactly the problem of non-interacting particles, which in this case are electrons (fermions). Next, the Coulomb interaction between electrons is introduced as a perturbation, which can be done by diagrammatic techniques such as the one developed by Feynman.

The electron-electron interaction is not a small term. Therefore, a few terms in the perturbative expansion will not solve the problem. It is necessary to consider infinite sums of

perturbative terms of certain classes (re-summations), which are expected to be the most relevant ones. Hartree-Fock approximation is one of these cases, where only two tipes of diagram are retained, direct Coulomb and exchange. The random phase-approximation (RPA) is another possible re-summation of diagrams that begins from the non-interacting electron system as a reference.

However, a system of non-interacting electrons is not necessarily the best possible starting point for which the exact solution is available. In fact, the Hartree-Fock approximation can be solved exactly or at least to an excellent extent using several computational approaches.

Møller-Plesset theory

Another option is to take the sum of Fock operators ($\hat{F}_i$) as the reference Hamiltonian for a perturbative expansion [64],

$$\hat{H}_0 = \sum_{i=1}^{N} \hat{F}_i = \sum_{i=1}^{N} \left[\hat{H}_0(i) + \sum_{k=1}^{N} \left(\hat{V}_{ik} - \hat{V}_{ijk} \right) \right]. \tag{2.66}$$

This has the advantage that the unperturbed eigenstates are the well-known Hartree-Fock determinants, which are far closer to the exact solution than the non-interacting system. In this case the perturbation takes the form

$$\Delta\hat{H} = \frac{1}{2} \sum_{i \neq j} V(i,j) - \sum_{ik} \left(\hat{V}_{ik} - \hat{V}_{ijk} \right). \tag{2.67}$$

This theory was developed in 1934 by Møller and Plesset, and is called Møller-Plesset (MP) perturbation theory. The unperturbed energies are just the sum of the eigenvalues of the Fock operator over all the occupied states

$$E_{MP}^{(0)} = \sum_{i=1}^{N} E_i, \tag{2.68}$$

and the first order energy, i.e. the sum of the unperturbed energy and the first order correction, is the Hartree-Fock energy

$$E_{MP1} = E_{MP}^{(0)} + E_{MP}^{(1)} = \sum_{i=1}^{N} E_i + \frac{1}{2} V_{ee} - V_{ee} = \sum_{i=1}^{N} E_i - \frac{1}{2} V_{ee} = E_{HF}, \tag{2.69}$$

where V_{ee} is the electrostatic energy calculated as the expectation value of the two-body Coulomb operator in the unperturbed Hartree-Fock state $\Psi_k^{(0)}$,

$$V_{ee} = \left\langle \Psi_k^{(0)} \middle| \sum_{i \neq j} V(i,j) \middle| \Psi_k^{(0)} \right\rangle . \tag{2.70}$$

The Hartree-Fock ground state corresponds to $k = 0$.

The first non-trivial correction is to second order (MP2), which involves matrix elements of $\Delta\hat{H}$ between the Hartree-Fock reference state and all the excited states constructed as in a CI expansion. Since $\Delta\hat{H}$ is a two-body operator, the only excited states contributing a non-zero matrix element are the double excitations, this is a very useful property. Therefore, the first energy correction involving correlation is

$$E_{MP}^{(2)} = \sum_{\mu<\nu=N_{occ}+1}^{ND} \sum_{i<j=1}^{N_{occ}} \frac{\left| \left\langle \Psi_k^{(0)} \middle| \Delta\hat{H} \middle| \Psi_k^{ij\mu\nu} \right\rangle \right|^2}{E_k^{(0)} - E_k^{ij\mu\nu}}, \tag{2.71}$$

where electrons in the unperturbed many-body state k that occupy the orbitals i and j are promoted to the empty orbitals μ and ν.

The sum of this term to the Hartree-Fock energy is known as the MP2 energy,

$$E_{MP2} = E_{MP}^{(0)} + E_{MP}^{(1)} + E_{MP}^{(2)}. \tag{2.72}$$

The MP2 approximation consists of truncating the perturbative expansion for the energy at this level while correcting the wave functions to first order. The scaling of the MP2 method with the number of basis functions (M) is of order M^5. For small systems (around 10 atoms), the cost of the MP2 correction is comparable to that of a Hartree-Fock calculation, although the more unfavorable scaling results more expensive for larger systems.

Higher orders in the perturbation expansion can also be included, and may be less expensive than CI calculations. The energy at the MP3 level can be calculated using the first order corrected wave functions, by the $2n+1$ theorem. Therefore, MP3 also involves only double excitations, but the doubles interact between themselves. The scaling is of the order M^6, and it recovers $90-95\%$ of the correlation energy. This is consistent with the observation that double excitations are energetically the most important ones. The next level in perturbation theory is MP4, which

involves single, double, triple, and quadruple excitations, and scales like M^7. The cost of an MP4 calculation is similar to that of CISD, and it accounts for $95-98\%$ of the correlation energy.

The MP2 approximation is the way of choice in quantum chemical calculations whenever low-level electronic correlation is required. It is the least expensive correlated method, and rather accurate as it tipically recovers around $80-90\%$ of the correlation energy. The remainder is important when the system consists of weakly interacting fragments. In fact, MP2 does not reproduce the correct dissociation limit, this requires at least an MP4 calculation. Unlike the CI expansion, perturbative methods are not variational, so that the energy may be lower than the exact energy.

The main limitation of the MP method is that it relies on a Hartree-Fock reference state. If Hartree-Fock provides a poor description of the system, then the correction terms are larger and the perturbation expansion requires more terms to be accurate.

Coupled clusters

Quantum many-body perturbation expansions can be considered to include an infinite number of terms of a certain class, while discarding all the terms of other type. This idea was proposed in 1989 by Bartlett and it is known as *coupled clusters* (CC) [64]. In this method the wave function is written as

$$\Psi_{cc} = e^{\hat{T}}\Psi_0, \tag{2.73}$$

where Ψ_0 is the Hartree-Fock wave function and $\hat{T} = \hat{T}_1 + \hat{T}_2 + \cdots + \hat{T}_N$ is an operator acting on the Hartree-Fock wave function that has the effect of generating all the excited Slater determinants up to certain order. In fact, single excitations corresponds to the first term,

$$\hat{T}_1\Psi_k^{(0)} = \sum_{\mu=N_{occ}+1}^{ND}\sum_{i=1}^{N_{occ}} t_i^{\mu}\Psi_k^{i\mu}, \tag{2.74}$$

while the second term,

$$\hat{T}_2\Psi_k^{(0)} = \sum_{\mu<\nu=N_{occ}+1}^{ND}\sum_{i<j=1}^{N_{occ}} t_{ij}^{\mu\nu}\Psi_k^{ij\mu\nu}, \tag{2.75}$$

includes double excitations, and so on. The coefficients t are equivalent to the coefficient C in the CI expansion.

By expanding the exponential,

$$e^{\hat{T}} = \hat{I} + \hat{T}_1 + \left(\hat{T}_2 + \frac{1}{2}\hat{T}_1^2\right) + \left(\hat{T}_3 + \hat{T}_2\hat{T}_1 + \frac{1}{6}\hat{T}_1^3\right) + \cdots , \tag{2.76}$$

it can be seen that the CC wave function includes all the excited Slater determinants.

Using the above wave function, the Schrödinger equation reads

$$\hat{H}\left(e^{\hat{T}}\Psi_0\right) = E_{cc}\left(e^{\hat{T}}\Psi_0\right), \tag{2.77}$$

and the corresponding energy is

$$E_{cc} = \langle \Psi_0 | \hat{H} e^{\hat{T}} | \Psi_0 \rangle . \tag{2.78}$$

Using the fact that the Hamiltonian contains only one- and two-body operators, it turns out that the CC energy is given exactly in terms of singles and doubles, in the following form

$$E_{cc} = E_{HF} + \sum_{\mu<\nu=N_{occ}+1}^{ND} \sum_{i<j=1}^{N_{occ}} \left(t_{ij}^{\mu\nu} + t_i^{\mu} t_j^{\nu} - t_i^{\nu} t_j^{\mu}\right) \langle \Psi_0 | \Delta\hat{H} | \Psi^{ij\mu\nu} \rangle , \tag{2.79}$$

where the coefficients t_i^{μ} and $t_{ij}^{\mu\nu}$ are determined by solving CI-type equations derived from the expansion of the exponential. Keeping all orders in this hierarchy is equivalent to full CI, and it is practically impossible. Truncated expansions are used in the same spirit of CI calculations. Choosing $\hat{T} = \hat{T}_2$ leads to the CCD level of approximation, and using $\hat{T} = \hat{T}_1 + \hat{T}_2$ corresponds to the CCSD level of approximation. The computational cost scales like M^6 as an MP3 calculation. When the $\hat{T}_3$ operator is included, the scaling becomes M^8, and it is more demanding than a CISDT calculation. CCSD is as costly as CISD, but the re-summation involved makes it more accurate. In fact, CCSD is as accurate as MP4, but at a significantly lower cost.

2.4 Perturbation theory

Time-independent perturbation theory

Is an approximate method to solve the Schrödinger equation of a many-body system, and obtain its response in the presence of a time-independent external field (electric or magnetic), as long as this field is not too large. In this case, the problem can be regarded as the Hamiltonian of the system without an external field $\hat{H}_0$ perturbed by the external field. It is expected that energy

levels and eigenfunctions of $\hat{H}$ are approximately those of $\hat{H}_0$ with small corrections due to the perturbation.

The Hamiltonian of the problem can be written as

$$\hat{H} = \hat{H}_0 + \hat{V}, \tag{2.80}$$

where $\hat{V}$ is the perturbation potential, which may depend on the position and other operators. Therefore, the equation that must be solved is the time-independent Schrödinger equation

$$\hat{H}\Psi_n = (\hat{H}_0 + \hat{V})\Psi_n = E_n\Psi_n. \tag{2.81}$$

The solutions of the unperturbed stationary problem are known

$$\hat{H}_0\psi_n = E_n^{(0)}\psi_n, \tag{2.82}$$

where $E_n^{(0)}$ are the eigenvalues of the Hamiltonian $\hat{H}_0$.

Eigenfunctions Ψ_n can be expressed as

$$\Psi_n = \psi_n + \phi_n, \tag{2.83}$$

where ϕ_n is the modification of the wave function due to the small perturbation. Since ϕ_n is not known, it is possible to use the unperturbed eigenfunctions ψ_n as a basis to develop ϕ_n

$$\Psi_n = \psi_n + \sum_k C_{nk}\psi_k. \tag{2.84}$$

By substituting Eq. (2.84) into Eq. (2.81)

$$(\hat{H}_0 + \hat{V})\left[\psi_n + \sum_k C_{nk}\psi_k\right] = E_n\left[\psi_n + \sum_k C_{nk}\psi_k\right] \tag{2.85}$$

and subtracting Eq. (2.82) yields

$$\sum_k C_{nk}E_k^{(0)}\psi_k + \hat{V}\psi_n + \sum_k C_{nk}\hat{V}\psi_k = \sum_k C_{nk}E_n^{(0)}\psi_k + \delta E_n\psi_n + \delta E_n\sum_k C_{nk}\psi_k, \tag{2.86}$$

where

$$\delta E_n = E_n - E_n^{(0)}. \tag{2.87}$$

Multiplying Eq. (2.86) by ψ_l^* and integrating gives

$$\sum_k V_{lk}C_{nk} + V_{ln} - (E_n^{(0)} - E_l^{(0)} + \delta E_n)C_{nl} = \delta E_n \delta_{nl}, \tag{2.88}$$

where $V_{nl} = \langle n | \hat{V} | l \rangle$ are the matrix elements of the perturbation potential.

Equation (2.88) is a system of equations for the energy corrections δE_n and for the wave function (2.84) expansion coefficients C_{nl}. In general, it is not possible to solve this system in an exact way.

By taking $l = n$ in Eq. (2.88) gives

$$\sum_k V_{nk}C_{nk} + V_{nn} - \delta E_n C_{nn} = \delta E_n. \tag{2.89}$$

From the sum the term $k = n$ is extracted, and solving for δE_n gives

$$\delta E_n = V_{nn} + \frac{\sum_k' V_{nk}C_{nk}}{1 + C_{nn}}. \tag{2.90}$$

Equation (2.90) shows that the perturbation effects are manifested directly in the system energy.

Next, by taking $l \neq n$ into Eq. (2.88) and substituting Eq. (2.90) yields

$$\sum_{k\neq n,l} V_{lk}C_{nk} + (1 + C_{nn})V_{ln} - \left(E_n^{(0)} - E_l^{(0)} + V_{nn} - V_{ll} + \frac{\sum_k' V_{nk}C_{nk}}{1 + C_{nn}} \right) C_{nl} = 0. \tag{2.91}$$

This nonlinear system of equations allows to determine the coefficients C_{nl} for $n \neq l$. In order to determine C_{nn}, the wave function Ψ_n must be normalized to unity, i.e.,

$$\langle \Psi_n | \, \Psi_n \rangle = 1 + C_{nn} + C_{nn}^* + \sum_k |C_{nk}|^2 = 1, \tag{2.92}$$

which is equivalent to

$$|C_{nn}|^2 + 2ReC_{nn} + \sum_k{}' |C_{nk}|^2 = 0, \tag{2.93}$$

the solution for C_{nn} in the Eq. (2.93) is

$$1 + C_{nn} = \sqrt{1 - \sum_k{}' |C_{nk}|^2}. \tag{2.94}$$

Equations (2.91) and (2.94) determine the expansion coefficients C_{nl}, so wave functions and energy eigenvalues can be determined with them. Because the previous system of equations is quite complex, it is necessary to use an approximated solution.

The expansion coefficients C_{nl} and energy corrections δE_n can be expressed as the sum of first, second, ... order contributions, using the auxiliar parameter λ as follows

$$\begin{aligned} C_{nl} &= \lambda C_{nl}^{(1)} + \lambda^2 C_{nl}^{(2)} + \lambda^3 C_{nl}^{(3)} + \cdots \\ \delta E_n &= \lambda \delta E_n^{(1)} + \lambda^2 \delta E_n^{(2)} + \lambda^3 \delta E_n^{(3)} + \cdots \end{aligned} \tag{2.95}$$

where λ^k factors indicate the smallness order of the corresponding term. By substituting Eq. (2.95) into Eq. (2.94) and matching the coefficients of each power of λ in both sides of the equation, yields

$$\begin{aligned} C_{nn}^{(1)} &= 0, \\ C_{nn}^{(2)} &= -\frac{1}{2} \sum_k{}' |C_{nk}^{(1)}|^2. \end{aligned} \tag{2.96}$$

This result shows that there is no correction to the coefficients C_{nn} at first order, but it exists to higher orders.

In order to obtain the energy corrections to different orders, Eqs. (2.95) and (2.96) are substituted into Eq. (2.90), and the coefficients of each power of λ are matched

$$\delta E_n^{(1)} = V_{nn}, \tag{2.97}$$

$$\delta E_n^{(2)} = \sum_k{}' C_{nk}^{(1)} V_{nk}. \tag{2.98}$$

Equation (2.97) is the most important result of the perturbation theory, since it indicates that the energy correction to first order is given by the expectation value of the perturbation Hamiltonian calculated with the unperturbed wave function of the corresponding state.

To determine the corrections to the wave functions, the Eqs. (2.95) and (2.98) are substituted into Eq. (2.91), and the coefficients of each power of λ must be canceled, which results in the following system of equations

$$\begin{aligned} V_{ln} - (E_n^{(0)} - E_l^{(0)}) C_{nl}^{(1)} &= 0, \\ \sum_{k \neq n,l} V_{lk} C_{nk}^{(1)} - (E_n^{(0)} - E_l^{(0)}) C_{nl}^{(2)} - (V_{nn} - V_{ll}) C_{nl}^{(1)} &= 0. \end{aligned} \tag{2.99}$$

The previous system of equations is solved and the corrections to the coefficients C_{nl} to first and second order are obtained

$$C_{nl}^{(1)} = \frac{V_{ln}}{E_n^{(0)} - E_l^{(0)}}, \tag{2.100}$$

$$C_{nl}^{(2)} = \frac{\sum_{k\neq n,l} V_{lk}C_{nk}^{(1)} - (V_{nn} - _{ll})C_{nl}^{(1)}}{E_n^{(0)} - E_l^{(0)}}. \tag{2.101}$$

Equations (2.100) and (2.101) allow to calculate the wave functions to first and second order in the time-independent perturbation theory.

Time-dependent perturbation theory

Previously the static case was considered, in which the perturbation potential does not depend on time, in this case the time-dependent Schrödinger equation (2.21) can be solved using the method of separation of variables, obtaining

$$\Psi(\mathbf{r}, t) = \psi(\mathbf{r})e^{-iEt/\hbar}, \tag{2.102}$$

where $\psi(\mathbf{r})$ satisfies the time-independent (or the eigenvalue) Schrödinger equation ($H\psi = E\psi$).

In order to take into account transitions between two energy levels, it is necessary to introduce a time-dependent potential (quantum dynamics) [68]. If the time-dependent portion of the Hamiltonian is small compared with the time-independent part, it can be treated as a perturbation.

The general solution of the unperturbed problem

$$i\hbar\frac{\partial\psi^{(0)}}{\partial t} = \hat{H}_0\psi^{(0)} \tag{2.103}$$

can be expressed as

$$\psi^{(0)}(\mathbf{r}, t) = \sum_k C_k e^{-iE_k t/\hbar}\phi_k(\mathbf{r}), \tag{2.104}$$

where ϕ_k are the eigenfunctions of $\hat{H}_0$, and E_k are the corresponding eigenvalues. The coefficients C_k are given by

$$C_k = \int \phi_k^*(\mathbf{r})\psi^{(0)}(\mathbf{r}, t = 0)d\mathbf{r}. \tag{2.105}$$

To solve Eq. (2.21) the Dirac's variation of constants method is used, which consists of write the solutions in the form (2.104) but with the coefficients C_k as functions of time

$$\Psi(\mathbf{r}, t) = \sum_k C_k(t)e^{-iE_k t/\hbar}\phi_k(\mathbf{r}). \tag{2.106}$$

By substituting Eq. (2.106) into Eq. (2.21), is obtained

$$i\hbar \sum_k \dot{C}_k(t) e^{-iE_k t/\hbar} \phi_k(\mathbf{r}) = \sum_k C_k(t) e^{-iE_k t/\hbar} \hat{H}^{(1)}(\mathbf{r}, t) \phi_k(\mathbf{r}), \tag{2.107}$$

Eq. (2.107) is multiplied by ϕ_l^* and is integrated over all space to obtain

$$\dot{C}_l(t) = -\frac{i}{\hbar} \sum_k C_k(t) e^{i(E_l - E_k)t/\hbar} H_{lk}^{(1)}, \tag{2.108}$$

where $H_{lk}^{(1)}$ are the matrix elements of the perturbation Hamiltonian.

Assuming that the perturbation is applied at $t = 0$. By integrating Eq. (2.108) over time, is obtained

$$C_l(t) = C_l(0) - \frac{i}{\hbar} \sum_k \int_0^t C_k(t') e^{i\omega_{lk} t'} H_{lk}^{(1)} dt', \tag{2.109}$$

where

$$\omega_{lk} = \frac{E_l - Ek}{\hbar}. \tag{2.110}$$

The inicial value $C_l(0)$ is obtained from Eq. (2.105)

$$C_l(0) = \int \phi_l^*(\mathbf{r}) \psi^{(0)}(\mathbf{r}, t = 0) d\mathbf{r}. \tag{2.111}$$

Assuming that before the perturbation the system is in an eigenstate of $\hat{H}_0$ (named as ϕ_n). Therefore, $\psi^{(0)}(\mathbf{r}, t = 0) = \phi_n(\mathbf{r})$, and by substituting it into Eq. (2.111) yields

$$C_l(0) = \delta_{ln}. \tag{2.112}$$

It is appropriate designate the wave function that is searched for as $\Psi_n(\mathbf{r}, t)$, therefore, the index n is added to the expansion coefficients into Eq. (2.106), thus obtaining

$$\Psi_n(\mathbf{r}, t) = \sum_k C_{nk}(t) e^{-iE_k t/\hbar} \phi_k(\mathbf{r}). \tag{2.113}$$

In order to solve the exact system of integral equations (2.109), a perturbation expansion to the coefficients C_{nk} is performed

$$C_{nk}(t) = C_{nk}(0) + C_{nk}^{(1)}(t) + C_{nk}^{(2)}(t) + \cdots \tag{2.114}$$

By substituting Eq. (2.114) into Eq. (2.109) and taking into account that $C_{nk}(0) = \delta_{nk}$ gives

$$\begin{aligned} C_{nl}(0) + C_{nl}^{(1)}(t) + C_{nl}^{(2)}(t) + \cdots &= C_{nl}(0) - \frac{i}{\hbar}\int_0^t e^{i\omega_{ln}t'} H_{ln}^{(1)} dt' \\ &\quad -\frac{i}{\hbar}\sum_k \int_0^t (C_{nk}^{(1)}(t') + \cdots) e^{i\omega_{lk}t'} H_{lk}^{(1)} dt'. \end{aligned} \tag{2.115}$$

Hence, the coefficients $C_{nl}(t)$ to first and second order are

$$C_{nl}^{(1)}(t) = C_{nk}^{(1)}(t) = -\frac{i}{\hbar}\int_0^t e^{i\omega_{kn}t'} H_{kn}^{(1)}(t') dt', \tag{2.116}$$

$$\begin{aligned} C_{nl}^{(2)}(t) &= -\frac{i}{\hbar}\sum_k \int_0^t (C_{nk}^{(1)}(t') + \cdots) e^{i\omega_{lk}t'} H_{lk}^{(1)}(t') dt' \\ &= \left(-\frac{i}{\hbar}\right)^2 \sum_k \int_0^t \int_0^{t'} e^{i\omega_{lk}t'} H_{lk}^{(1)}(t') e^{i\omega_{kn}t''} H_{kn}^{(1)}(t'') dt'' dt'. \end{aligned} \tag{2.117}$$

Equation (2.117) shows that by applying the perturbation, transitions occur toward states conected with the initial state through the perturbation potential matrix or its products.

The transition probability is obtained as follows

$$P_{nk}(t) = |C_{nk}(t)|^2. \tag{2.118}$$

The previous equation is the probability that a particle which is initially in the n state is found in the k state, at time t.

2.5 Density Functional Theory

L. H. Thomas and E. Fermi proposed, at about the same time as Hartree (1927-1928), that the full electronic density was the fundamental variable of the many-body problem. They derived a differential equation for the density without resort to one-electron orbitals. The original Thomas-Fermi approximation used for the kinetic energy of the electrons was unable to sustain bound states. However, it established the basis for the later development of density functional theory (DFT), which is used in electronic structures calculations in condensed matter physics during the past twenty years and, recently, has been accepted by the quantum chemistry community because of its computational advantages compared to Hartree-Fock methods [64].

Thomas (1927), and independently Fermi (1928), proposed to calculate the energy of an electronic system only in terms of the electronic density. In their original work Thomas and Fermi proposed an expression for the total electronic energy where the kinetic, exchange, and correlation contributions were taken from the homogeneous electron gas, for which good approximations were known. The idea was to construct the same quantities for the inhomogeneous system as [64]

$$E_\alpha[\rho] = \int \rho(\mathbf{r})\epsilon_\alpha[\rho(\mathbf{r})]d\mathbf{r}, \tag{2.119}$$

where $\epsilon_\alpha[\rho(\mathbf{r})]$ is the energy density of contribution α (kinetic, exchange, and correlation), calculated locally at the value assumed by the density at every point in space. This was the first time that the local density approximation was proposed.

For an ideal gas (homogeneous, without particle interactions), the average kinetic energy in the ground state is [71]

$$KE = \frac{3}{5}E_F = \frac{3\hbar^2 k_F^2}{10m}, \tag{2.120}$$

where

$$k_F = (3\pi^2\rho_0)^{1/3} \tag{2.121}$$

k_F is the Fermi wave vector, and ρ_0 is the uniform density.

The Thomas-Fermi approximation assumes that this relation is also valid for nonuniform systems [71]

$$k_F(\mathbf{r}) = (3\pi^2\rho(\mathbf{r}))^{1/3}, \tag{2.122}$$

$$KE(\mathbf{r}) = \frac{3}{5}(3\pi^2\rho(\mathbf{r}))^{2/3}Ry. \tag{2.123}$$

All the energy units are Rydbergs ($Ry = e^2/2a_0$), and all of the distances are given in terms of the Bohr radius ($a_0 = \hbar^2/me^2$). The expression for the kinetic energy given by Eq. (2.123) is a function of position. Its contribution to the ground state energy is obtained by integrating this expression over the volume, weighting each point with the particle density [71]

$$T_s = \int \rho(\mathbf{r})KE(\mathbf{r})d^3r \tag{2.124}$$

$$= \frac{3}{5}(3\pi^2)^{2/3}\int \rho(\mathbf{r})^{5/3}d^3r. \tag{2.125}$$

A first attempt at constructing a functional of the ground state energy is

$$E_{TF}\left[\rho\right] = \frac{3}{5}(3\pi^2)^{2/3}\int \rho(\mathbf{r})^{5/3}d^3r + \int \rho(\mathbf{r})U(\mathbf{r})d^3r + \int \frac{\rho(\mathbf{r}_1)\rho(\mathbf{r}_2)}{|\mathbf{r}_1-\mathbf{r}_2|}d^3r_1d^3r_2, \tag{2.126}$$

where $U(\mathbf{r})$ is an external potential.

Now taking the functional derivative of the ground state energy with respect to the density, with the constraint that the number of electrons does not change. This constraint is introduced using Lagrange multipliers,

$$\frac{\delta}{\delta\rho(\mathbf{r})}\left[E_{TF}[\rho] - \mu\int \rho(\mathbf{r})d^3r\right] = 0, \tag{2.127}$$

$$\mu = \left[3\pi^2\rho(\mathbf{r})\right]^{2/3} + U(\mathbf{r}) + 2\int \frac{\rho(\mathbf{r}')}{|\mathbf{r}-\mathbf{r}'|}d^3r', \tag{2.128}$$

where μ is the chemical potential.

Equation (2.128) can be solved to obtain the density as a function of the screened potential

$$\rho(\mathbf{r}) = \frac{1}{3\pi^2}\left\{\mu - U(\mathbf{r}) - V_H\left[\rho(\mathbf{r})\right]\right\}^{3/2}, \tag{2.129}$$

where

$$V_H\left[\rho(\mathbf{r})\right] = 2\int \frac{\rho(\mathbf{r}')}{|\mathbf{r}-\mathbf{r}'|}d^3r'. \tag{2.130}$$

$V_H\left[\rho(\mathbf{r})\right]$ is the Hartree potential, and is a density functional, since the Eq. (2.31) can be expressed in terms of the charge density $\rho(\mathbf{r_l}) = e^2\varphi(\mathbf{r}_l)^*\varphi(\mathbf{r}_l)$.

Then, the Poisson's equation is obtained [71]

$$\nabla^2 V_H\left[\rho(\mathbf{r})\right] = -8\pi\rho(\mathbf{r}) \tag{2.131}$$

$$= -\frac{8}{3\pi}\left\{\mu - U(\mathbf{r}) - V_H\left[\rho(\mathbf{r})\right]\right\}^{3/2}. \tag{2.132}$$

This result is the Thomas-Fermi equation. This result is numerically not very accurate and, in order to improve it, the kinetic energy term must be optimized. Improvements can be achieved by introducing terms which involve the gradient of the density. Moreover, a better result can be accomplished by introducing other terms. The modern theory uses the form for the kinetic energy in terms of wave functions (as will be described in section 2.4.2). Additional improvements in the ground state energy are achieved by introducing terms which take into account the effects of exchange and correlation.

The Hohenberg-Kohn theorem

The Thomas-Fermi approximation was developed with the aim of write the kinetic energy in terms of the electronic density. However, this idea was intuitive at the time, and took more than thirty years to prove this theory. In 1964, Hohenberg and Kohn formulated and proved a theorem that put on solid mathematical grounds the previous ideas. The theorem is divided in two parts.

Theorem 1. The external potential is univocally determined by the electronic density, besides a trivial additive constant [64]. This means that cannot be $U(\mathbf{r}) \neq U^{'}(\mathbf{r})$ that correspond to the same electronic density for the ground state, unless they differ by a trivial additive constant.

Since $\rho(\mathbf{r})$ univocally determines $U(\mathbf{r})$, it also determines the ground state wave function Φ, which should be obtained by solving the many-body Schrödinger equation.

Theorem 2. Let $\tilde{\rho}(\mathbf{r})$ be a non-negative density normalized to N. A variational energy E_v is defined, which is a functional of the density because of the previous theorem, $E_v\left[\tilde{\rho}\right]$. So that $E_0 = E_v\left[\rho\right]$ verifies

$$E_0 < E_v\left[\tilde{\rho}\right], \tag{2.133}$$

for any $\tilde{\rho} \neq \rho$, and is thus the ground state energy [64].

These two theorems form the mathematical basis of DFT.

The Kohn-Sham equations

It is possible to separate the classical electrostatic energy (the Hartree term) from the exchange and correlation contributions. This strategy is useful because it divides the generally unknown electron-electron interaction energy into parts of decreasing importance from the energetic point of view: Hartree, exchange, and correlation. The Hartree term is by far the largest contribution, is the classical electrostatic energy, which is known. The exchange term (the second largest) is also known and, in principle, can be calculated exactly as in the Hartree-Fock theory. However, in practice, for computational reasons, this term is approximated. The correlation term (the smallest contribution) is the biggest difficulty. In fact, this is an active field of research, which has produced significant improvements over the past decades [64].

The main problem here is with the kinetic energy term, because its explicit expression in terms of the electronic density is not known. A more general approach was suggested by Kohn and Sham (1965), they introduced several more features to DFT which brought it to the form which is used today. Their theory is called Local Density Approximation.

The Kohn-Sham treatment of the kinetic energy term consists of using the expression for the kinetic energy in terms of wave functions (in atomic units) [71]

$$T_s = \int \sum_j \nabla \psi_j^\dagger \cdot \nabla \psi_j d^3 r, \tag{2.134}$$

this equation corresponds to the kinetic energy of a non-interacting particle system.

The ground state energy is the sum of the kinetic energy term plus the external potential and Hartree terms, as well as an exchange-correlation term [71]

$$E_G\left[\rho\right] = T_s + E_{xc} + \int \rho(\mathbf{r}) U(\mathbf{r}) d^3 r + \int \frac{\rho(\mathbf{r}_1)\rho(\mathbf{r}_2)}{|\mathbf{r}_1 - \mathbf{r}_2|} d^3 r_1 d^3 r_2, \tag{2.135}$$

where

$$E_{xc} = E_x + E_c = \int \rho(\mathbf{r}) \epsilon_{xc}\left[\rho(\mathbf{r})\right] d^3 r. \tag{2.136}$$

$\epsilon_{xc}\left[\rho(\mathbf{r})\right]$ is the ground state exchange-correlation energy per electron.

Taking a functional derivative of the ground state energy, in this case the variation is with respect to the Hermitian conjugate of the eigenfunction $\psi_j^\dagger$, with the constraint that the number of particles is preserved. This step introduces the Lagrange multiplier λ,

$$\frac{\delta}{\delta \psi_j^\dagger}\left[E_G - \lambda \int \rho(\mathbf{r}) d^3 r\right] = 0. \tag{2.137}$$

The functional derivative of the terms in Eq. (2.135), except for the kinetic energy term, is performed as follows

$$\frac{\delta E}{\delta \psi_j^\dagger} = \frac{\delta E}{\delta \rho(\mathbf{r})} \frac{\delta \rho(\mathbf{r})}{\delta \psi_j^\dagger}, \tag{2.138}$$

where E corresponds to each term of Eq. (2.135) except T_s.

The result of Eq. (2.137) is [71]

$$\left[-\nabla^2 + U(\mathbf{r}) + V_H\left[\rho(\mathbf{r})\right] + V_{xc}\left[\rho(\mathbf{r})\right]\right] \psi_j = \lambda_j \psi_j, \tag{2.139}$$

where $V_H[\rho(\mathbf{r})]$ is given by Eq. (2.130), and $V_{xc}[\rho(\mathbf{r})]$ is

$$V_{xc}[\rho(\mathbf{r})] = \frac{\delta E_{xc}}{\delta \rho(\mathbf{r})}. \tag{2.140}$$

The density is obtained by summing over the N lowest eigenfunctions, where N is the total number of electrons,

$$\rho(\mathbf{r}) = \sum_{j}^{N} |\psi_j(\mathbf{r})|^2. \tag{2.141}$$

Equations (2.139) are known as Kohn-Sham equations, this set of equations is a self-consistent way of solving for the ground state energy. First an initial density is proposed, and by using this density the Kohn-Sham equations are solved for the eigenfunction ψ_j for each occupied state j, these eigenfunctions are used to calculate a new electronic density, and this density is used to obtain the potential terms. The process is repeated until convergence is achieved. In the Kohn-Sham equations, ψ_j represents a wave function of a virtual electron that moves in a potential $\left[-\nabla^2 + U(\mathbf{r}) + V_H[\rho(\mathbf{r})] + V_{xc}[\rho(\mathbf{r})]\right]$.

As a result of this calculation two important quantities are obtained: the electronic density $\rho(\mathbf{r})$, and the ground state energy E_G. The ground state energy is calculated easily after achieving self-consistency in the eigenfunctions. Since the density is given by Eq. (2.141), it is possible to rewrite the ground state energy, after an integration by parts in the kinetic energy, as

$$E_G = \sum_{j} \int \psi_j^{\dagger} \left[-\nabla^2 + U(\mathbf{r}) + \frac{1}{2} V_H[\rho(\mathbf{r})] + \epsilon_{xc}[\rho(\mathbf{r})]\right] \psi_j d^3r. \tag{2.142}$$

In the Kohn-Sham equations ψ_j and λ_j are known as Kohn-Sham eigenfunction and Kohn-Sham eigenvalue, respectively. These quantities do not have a rigorous physical interpretation, they are just quantities obtained to solve the equations, i.e., λ_j does not represent the energy levels for single electrons. The only quantities that have a physical interpretation are the ground state energy E_G and the electronic density $\rho(\mathbf{r})$, and both can be, in principle, measured experimentally.

B3LYP functional

In this work the Becke's hybrid functional with three parameters and Lee-Yang-Parr functional (B3LYP) was used, because this functional performs significantly better than other functionals

with gradient corrections only, and fits experimental values for the case of BNNT (see Chapter 3).

This functional was proposed by Becke in 1993 [72]. Despite the well-intentioned efforts of density-functional researchers to circumvent the calculation of exact-exchange energies, a small exact-exchange component is a natural and necessary constituent of any exchange-correlation approximation aiming for accurate molecular energies.

The exchange-correlation energy E_{xc} of Kohn-Sham DFT is given by a rigorous ab initio formula known as the "adiabatic connection" formula. One of the many possible forms that this important result may take is [72]

$$E_{xc} = \int_0^1 U_{xc}^{\lambda} d\lambda, \tag{2.143}$$

where λ is an interelectronic coupling-strength parameter that "switches on" the $1/r_{12}$ Coulomb repulsion between electrons, and U_{xc}^{λ} is the potential energy of exchange-correlation at intermediate coupling strength λ. This formula "connects" the noninteracting Kohn-Sham reference system (defined by $\lambda = 0$) to the fully interacting real system ($\lambda = 1$) through a continuum of partially interacting systems ($0 \leq \lambda \leq 1$), all of which share a common density (the density of the real, fully interacting system). Though the integrand of Eq. (2.143) refers explicitly to potential energy only, the kinetic part of the exchange-correlation energy is generated by the λ integration.

Careful consideration of the λ dependence of the integrand in Eq. (2.143) is important in understanding the successes and failures of density-functional theories. In particular, the $\lambda = 0$ lower limit, corresponding to the noninteracting Kohn-Sham reference system, is of major relevance. The exchange-correlation potential energy U_{xc}^{0} is the pure exchange energy of the Slater determinant of the Kohn-Sham orbitals, with no dynamical correlation at all. This Kohn-Sham exchange energy E_x is essentially equal in value to the conventional Hartree-Fock exchange energy.

The $\lambda = 0$ limit of the coupling-strength integration of Eq. (2.143) is the exact exchange. Therefore, the exact exchange energy play a role in highly accurate density-functional theories. Accordingly, Becke proposed the following exchange-correlation approximation [72]

$$E_{xc} = E_{xc}^{LSDA} + a_0 \left(E_x^{exact} - E_x^{LSDA} \right) + a_x \Delta E_x^{B88} + a_c \Delta E_c^{PW91}, \tag{2.144}$$

where a_0, a_x, and a_c are semiempirical coefficients to be determined by an appropriate fit to experimental data, E_x^{exact} is the exact exchange energy, ΔE_x^{B88} is Becke's 1988 gradient correction (to the Local Spin Density Approximation, LSDA) for exchange [73], and ΔE_c^{PW91} is the 1991 gradient correction for correlation of Perdew and Wang [74]. For the correlation component of the leading term E_{xc}^{LSDA} was used the electron-gas parametrization of Perdew and Wang [75].

Equation 2.144 is motivated by reasonable physical arguments. The second term replaces some electron-gas exchange with exact exchange to capture the proper small-λ limit of Eq. (2.143). The coefficient a_0 thus reflects the relative importance of a system's independent-particle character, or the rate of onset of correlation as λ increases from zero. The third and fourth terms allow optimum admixtures of exchange and correlation-type gradient corrections. The coefficient a_x has value less than unity, since the presence of the E_x^{exact} term reduces the need for the gradient correction ΔE_x^{B88}. Flexibility in the coefficient a_c is allowed as well.

This functional has been applied to the atoms and molecules of the Gaussian-1 database [72]. The semiempirical coefficients of Eq. (2.144) have been determined by Becke [72] using a linear least-squares fit to experimental values of atomization energies, ionization potentials, proton affinities, and total atomic energies. The resulting optimum values are a_0=0.20, a_x=0.72, a_c=0.81.

2.6 Van der Waals interactions

van der Waals (vdW) interactions, also known as London dispersion interactions, represent a complex benchmark in many-body theory that any correlation functional should address. The origin of the vdW interaction between two non-chemically bonded fragments is the coupling of the electric field generated by fluctuations in the electronic density of one fragment with the density of the other fragment. This is a dynamical correlation effect that the usual Local Density Approximation (LDA) and semi-local (general-gradient approximation, GGA) functionals cannot capture, and is not related to the exchange. At long distances the vdW interaction should approach the classical dipole-dipole interaction, which decays as $E_{vdW} = -C_6/R^6$. Dispersion interactions constitute a small but important component to the interatomic forces in molecular fluids and biological systems.

The exact density functional contains the vdW forces, but this exact functional is not known. However, there are approximations to incorporate the vdW forces. Commonly, the LDA and GGA are used. They depend on the density in local and semi-local ways, respectively, and they give no account of the nonlocal vdW interaction.

Today, there are proposals for how the vdW interactions can be treated in DFT, in particular at large separations. This proposals include van der Waals density functional [76], Tkatchenko and Scheffler approximation [77], DFT-D [78], etc.

Van der Waals Density Functional

Dion et al. [76] developed and applied a van der Waals density functional (vdW-DF) for general geometries. The vdW-DF procedure is

$$E_{xc}[\rho] = E_x^{GGA}[\rho] + E_c^{new}[\rho], \tag{2.145}$$

that is to take an appropriately selected GGA exchange functional, to develop a properly constructed nonlocal correlation functional that includes an account of vdW forces, and to perform calculations with some efficient and accurate electron-structure scheme. The computer resources required for vdW-DF are comparable to ordinary DFT. By using the functional derivative of $E_c^{new}[\rho]$ with respect to the density $\rho(r)$ as a component of the Kohn-Sham electron potential, the calculations are made fully self-consistent.

The correlation energy is split into shorter- and longer-ranged parts [76]

$$E_c[\rho] = E_c^0[\rho] + E_c^{nl}[\rho]. \tag{2.146}$$

The short-ranged term, $E_c^0[\rho]$, is evaluated in LDA, which implicitly uses the exact dielectric function. The longer-ranged term, $E_c^{nl}[\rho]$, depends nonlocally on the density and contains the principal vdW terms. It is also much smaller in magnitude and in positional sensitivity, so it can be evaluated with a lower accuracy. In particular, in the vdW-DF it is evaluated with a simple model dielectric function.

In the vdW-DF the key ingredients of the long-range term (nonlocal) part of the correlation

functional are the adiabatic-connection formula as the starting point, an approximate coupling-constant integration, which is exact for the asymptotic long-range vdW term, the use of an approximate dielectric function ϵ in a single-pole form, which is fully nonlocal and satisfies known limits, sum rules and invariances, whose pole position is scaled to give the exact electron-gas ground-state energy locally, including the appropriate gradient correction, and the lack of empirical or fitted parameters.

The coupling-constant (λ) integration in the nonlocal correlation term $E_c^{nl}[\rho]$ in Eq. (2.146) is performed by making a simple approximation [79]

$$(\epsilon - 1)_\lambda = \left[\frac{(\epsilon - 1)}{\lambda}\right]_{\lambda=1} \lambda, \tag{2.147}$$

as this can be shown to give the longest-range vdW terms exactly, if long-range "spectator" interactions are also left out of the dielectric function. For intermediate separations its accuracy is tested in a large number of applications and comparisons with accurate results of wave function methods and/or experimental results, when such results are available. While singular in the well-known asymptotic form at large separations, the vdW interaction given by vdW-DF at small separations gives a saturation of the interaction.

The form of the general-geometry functional for $E_c^{nl}[\rho]$ is [76]

$$E_c^{nl} = \frac{1}{2} \int \int n(r)\Phi(r, r')n(r')d^3r'd^3r, \tag{2.148}$$

where $\Phi(r, r') = \Phi(q(r), q(r'))$. The interaction kernel depends on the density and its gradient, $q(r) = q(n(r), \nabla n(r))$, and can be given a scalable form via

$$D = \frac{q + q'}{2}|r - r'|, \qquad \delta = \frac{1}{2}\frac{q - q'}{q + q'}, \qquad q = q(r), \qquad q' = q(r'). \tag{2.149}$$

The kernel Φ is attractive at large and intermediate effective distances D. At very large D values, it takes its proper asymptotic form, and it has an oscillation at short distances D.

The use of vdW-DF, along with future improvements, may be the way to proceed for calculating properties of vdW bound molecules that are too large for wave function based methods to be useful.

Tkatchenko and Scheffler approximation

Tkatchenko and Scheffler [77] developed a parameter-free method for an accurate determination of long-range vdW interactions from mean-field electronic structure calculations. This method relies on the summation of interatomic C_6 coefficients, derived from the electron density of a molecule or solid and accurate reference data for the free atoms.

A popular remedy for the missing vdW interaction in DFT currently consists of adding a pairwise interatomic C_6R^6 term (E_{vdW}) to the DFT energy [78, 80–83],

$$E_{vdW} = -\frac{1}{2}\sum_{A,B} f_{damp}\left(R_{AB}, R_A^0, R_B^0\right) C_{6AB} R_{AB}^{-6}, \tag{2.150}$$

where R_{AB} is the distance between atoms A and B, C_{6AB} is the corresponding C_6 coefficient, R_A^0 and R_B^0 are the vdW radii. The R_{AB}^{-6} singularity at small distances is eliminated by the short-ranged damping function $f_{damp}\left(R_{AB}, R_A^0, R_B^0\right)$. At the medium and short range, this approach can only work together with xc functionals that underestimate the binding energy. A serious deficiency of the C_6R^{-6} schemes is their empirical nature, since the parameters do not depend on the electronic structure, but are rather obtained by fitting to experimental C_6 coefficients and/or post-Hartee-Fock binding energy data. Furthermore, the damping function will also correct (of affect) other properties of the employed xc functional at short distances. Though a correction of present-day xc functionals is necessary, it is not satisfactorily handled by such an approach.

The Tkatchenko and Scheffler approximation consists of develop and assess a scheme to determine the C_6 coefficients and vdW radii from the mean-field ground-state electron density for molecules and solids. This approximation shows a mean absolute error of 5.5% for intermolecular C_6 coefficients on a database of experimental dipole oscillator strength distribution (DOSD) data of Meath and co-workers for 1225 intermolecular pairs [77]. The DOSD for a given molecule is the (differential) dipole oscillator strength df/dE, as a function of excitation energy E, from the electronic absorption threshold E_0 to very high energies. The critical idea of this method is to use the electron density to compute the relative and not the absolute polarizability of an atom in a molecule. The method includes charge polarization effects in a transparent way, as shown for different atomic hybridization states and hydrogen bonding.

The formula for C_{6AB} which depends only on homonuclear parameters C_{6AA}, C_{6BB}, α_A^0, and α_B^0 is [77]

$$C_{6AB} = \frac{2C_{6AA}C_{6BB}}{\left[\frac{\alpha_B^0}{\alpha_A^0}C_{6AA} + \frac{\alpha_A^0}{\alpha_B^0}C_{6BB}\right]}, \tag{2.151}$$

where α_A^0 and α_B^0 are the static polarizabilities of A and B, respectively. The accuracy of the free-atoms results is presumed to be better than 3% for α_A^0 and C_{6AA} for nonmetallic elements (1% for rare gases, alkalis, and alkaline earth atoms) [77]. Using these homonuclear values along with Eq. (2.151), is obtained a mean absolute relative error of just 2.7% on a database of 70 heteronuclear C_6 coefficients between light elements, rare gases, alkalis, and alkaline earth atoms from accurate many body calculations [84–86].

The effective coefficient C_{6AA}^{eff} for an atom in a molecule is [77]

$$C_{6AA}^{eff} = \frac{\eta_A^{eff}}{\eta_A^{free}}\left(\frac{\kappa_A^{free}}{\kappa_A^{eff}}\right)^2\left(\frac{V_A^{eff}}{V_A^{free}}\right)^2 C_{6AA}^{free}, \tag{2.152}$$

where κ_A^i is the proportionality constant between volume and polarizability for the free atom and atom in a molecule, η_A^{free} is the electron density of the free atom A. The proporcionality constant $\frac{\eta_A^{eff}}{\eta_A^{free}}\left(\frac{\kappa_A^{free}}{\kappa_A^{eff}}\right)^2$ is assumed to be unity and prove this choice to be remarkably good for a large variety of molecules [77].

Since the C_6 coefficients are additive, the intermolecular C_6 coefficient, C_6^{mol}, is given by the sum of all interatomic contributions

$$C_6^{mol} = \sum_{A\in M_1}\sum_{B\in M_2} C_{6AB}^{eff}, \tag{2.153}$$

where M_1 and M_2 refers to the first and the second molecule, respectively.

This accurate nonempirical method to obtain molecular C_6 coefficients from ground-state electron density and reference values for the free atoms, can also be used to improve the description of weakly bonded systems in DFT for a range of xc functionals.

DFT-D

Although today the most widely used theoretical approach to molecular structure, the DFT, includes electron correlation effects in an approximate manner, it is now clear that almost all

gradient-corrected density functionals are unable to describe dispersive interactions. Although this problem now has become a very active field of research, it seems to be very difficult to account for dispersion within the standard Kohn-Sham picture of DFT. These nonlocal, long-range electron correlations already appear for vanishing overlap only a tiny effect on the electron density of the fragments that is furthermore buried by the influences of the chemical environment.

In 2004 Grimme [78] proposed that a C_6R^{-6} type correction to DFT (named DFT-D) is indeed generally applicable, and that tailoring the mathematical form of the potential to specific systems is not necessary.

The dispersion corrected total energy is

$$E_{MF-D} = E_{MF} + E_{disp}, \tag{2.154}$$

where E_{MF} is the usual mean-field energy (i.e., Hartree-Fock or DFT) and E_{disp} is an empirical dispersion correction given by

$$E_{disp} = -s_6 \sum_{i=1}^{N_{at}-1} \sum_{j=i+1}^{N_{nat}} \frac{C_6^{ij}}{R_{ij}^6} f_{damp}(R_{ij}), \tag{2.155}$$

where N_{at} is the number of atoms in the system, C_6^{ij} denotes the dispersion coefficient for atom pair ij, s_6 is a global scaling factor and R_{ij} is the interatomic distance. E_{disp} is a model-dependent quantity with no real physical meaning. To avoid near-singularities for small R, a damping factor f_{damp} must be used which is given by [78]

$$f_{damp}(R) = \frac{1}{1 + e^{-\alpha(R/R_0 - 1)}}, \tag{2.156}$$

where R_0 is the sum of atomic vdW radii. Eq. (2.156) is chosen because it decays at small R fast enough to zero such that the dispersion corrections between atoms well below typical vdW distances are negligible and thus, "normal" bonds are not significantly affected by the correction. The value of $\alpha = 23$, which determines the steepness of the damping function is used as in previous work [80].

Different combination rules for the composed C_6^{ij} coefficients have been carefully tested for many complexes [78]. However, it turned out that the observed effects were always smaller than those introduced by the finite atomic orbital (AO) basis and the choice of the density functional.

Thus, further search for the optimum dispersion function in that direction seems not warranted, and finally, a simple average of the form

$$C_6^{ij} = 2\frac{C_6^i C_6^j}{C_6^i + C_6^j} \tag{2.157}$$

is used [78]. The atomic C_6 coefficients are taken from [80], but have been averaged over the possible hybridization states of the atoms. A distinction of different hybridization states would clearly improve the flexibility of the correction, but seems to be problematic in cases where the hybridization states of the atoms are not well defined. The errors due to the use of atomic instead of hybridization-dependent C_6 coefficients may be on the order of 10-20% of the binding energy when, for example, saturated and unsaturated hydrocarbons are compared.

Depending on the actual mean field (or density functional), the atomic C_6 coefficients are scaled by the factor s_6 to account for the different behavior of the intermolecular potential especially at intermediate distances.

In general, the accuracy of the DFT-D model for intermolecular distances is estimated to be about 5-10 pm for systems dominated by vdW interactions. The interaction energies are accurate to about 10-30% in most cases and the accuracy in general increases with the size of the systems [78].

From a practical point of view, there seem to be two major modes of operation for the DFT-D approach. First, large scale applications in, for example, supramolecular chemistry or biochemistry where both electrostatic and dispersive interactions are important now become possible. Second, the DFT-D data may serve as input for other theoretical models, or the optimized structures can be used as input for more accurate and systematically improvable ab initio calculations of the interaction energies.

DFT-D3

In this work was used the method DFT-D3, which is the refined DFT-D method regarding higher accuracy, broader range of applicability, and less empiricism.

Grimme et al. proposed in 2010 [87] a new version of DFT-D method. This new version is

called DFT-D3, and compared with the previous and other recent DFT-D implementations and variants [78, 82, 87], the current version has the following properties and advantages:

- It is less empirical, i.e., the most important parameters are computed from first-principles by standard Kohn-Sham DFT/Time dependent DFT.
- The approach is asymptotically correct with all density functionals for finite systems (molecules) or nonmetallic infinite systems. It gives the almost exact dispersion energy for a gas of weakly interacting neutral atoms and smoothly interpolates to molecular (bulk) regions.
- It provides a consistent description of all chemically relevant elements of the periodic system (nuclear charge from Z=1 to Z=94).
- Atom pair-specific dispersion coefficients and cutoff radii are explicitly computed.
- Coordination number (geometry) dependent dispersion coefficients are used that do not rely on atom connectivity information (differentiable energy expression). From a physical and conceptual perspective, this is the widest change compared to the previous DFT-D versions as until now the (atomic) dispersion parameters were completely system independent. This is a very drastic restriction as these values depend, e.g., on the hybridization state of the atom in the molecule. For the first time is considered a simple account for this effect, that is, however, only geometry but not electronic structure dependent in order to keep the numerical complexity low.
- It provides similar or better accuracy for "light" molecules and a strongly improved description of metallic and "heavier" systems.

The total DFT-D3 energy is given by [87]

$$E_{DFT-D3} = E_{KS-DFT} - E_{disp}, \tag{2.158}$$

where E_{KS-DFT} is the usual self-consistent Kohn-Sham energy as obtained from the chosen density functional and E_{disp} is the dispersion correction as a sum of two- and three-body energies,

$$E_{disp} = E^{(2)} + E^{(3)}, \tag{2.159}$$

with the most important two-body term given by

$$E^{(2)} = \sum_{AB} \sum_{n=6,8,10,\ldots} s_n \frac{C_n^{AB}}{r_{AB}^n} f_{d,n}(r_{AB}). \tag{2.160}$$

The first sum is over all atom pairs in the system, C_n^{AB} denotes the averaged (isotropic) nth-order dispersion coefficient (orders $n = 6, 8, 10, \ldots$) for atom pair AB, and r_{AB} is their internuclear distance. Global (density functional dependent) scaling factors s_n are adjusted only for n>6 to ensure asymptotic exactness which is fulfilled when the C_6^{AB} are exact. This is a fundamental difference to previous methods [78, 82], where, in general, s_6 was not equal to unity and only scaled asymptotic value is obtained.

In order to avoid near singularities for small r_{AB} and (mid-range) double-counting effects of correlation at intermediate distances, damping functions $f_{d,n}$ are used which determine the range of the dispersion correction. The chosen function turns out to be numerically stable and convenient also for higher dispersion orders [87]

$$f_{d,n}(r_{AB}) = \frac{1}{1 + 6(r_{AB}/(s_{r,n} R_0^{AB}))^{-\alpha_n}}, \tag{2.161}$$

where $s_{r,n}$ is the order-dependent scaling factor of the cutoff radii R_0^{AB}. It replaces s_6-scaling in previous DFT-D methods and is the main and most important parameter that has to be adjusted for each density functional. After some testing it was proposed to optimize only $s_{r,6}$ by a standard least-squares error fitting procedure and fix $s_{r,8}$ for all density functionals to unity [87]. The "steepness" parameters α_n are also not fitted but adjusted manually such that the dispersion correction is <1% of max($|E_{disp}|$) for typical covalent bond distances. This is achieved by setting $\alpha_6 = 14$ and by taking $\alpha_{n+2} = \alpha_n + 2$.

The dispersion coefficients are computed ab initio by time-dependent DFT employing known recursion relations for the higher-multipole terms. The starting point is the Casimir-Polder formula [87]

$$C_6^{AB} = \frac{3}{\pi} \int_0^\infty \alpha^A(i\omega)\alpha^B(i\omega) d\omega, \tag{2.162}$$

where $\alpha(i\omega)$ is the averaged dipole polarizability at imaginary grequency ω. The higher-order coefficients are computed recursively according to [87]

$$C_8^{AB} = 3C_6^{AB}\sqrt{Q^A Q^B}, \tag{2.163}$$

$$C_{10}^{AB} = \frac{49}{40}\frac{\left(C_8^{AB}\right)^2}{C_6^{AB}}, \tag{2.164}$$

and

$$C_{n+4} = C_{n-2}\left(\frac{C_{n+2}}{C_n}\right)^3, \tag{2.165}$$

with

$$Q^A = s_{42}\sqrt{Z^A}\frac{\langle r^4\rangle^A}{\langle r^2\rangle^A}. \tag{2.166}$$

In Eq. (2.166) $\langle r^4\rangle^A$ and $\langle r^2\rangle^A$ are simple multipole-type expectation values derived from atomic densities which are averaged geometrically to get the pair coefficients. This seems to be sufficiently accurate because the C_6 value in Eq. (2.163) is computed explicitly for the pair AB. The *ad hoc* nuclear charge dependent factor $\sqrt{Z^A}$ in Eq. (2.166) is found to be necessary in order to get consistent interaction energies also for the heavier elements. The factor s_{42} is redundant because the higher-order contributions in Eq. (2.160) are scaled individually for each density functional.

Although the C_6^{AB} values can be computed easily for any pair of free atoms by using Eq. (2.162) in principle, this would lead to a rather inconsistent treatment of dispersion in and between molecules. The polarizabilities of many atoms are strongly influenced by energetically low-lying atomic states (open valence shells) which leads to very large dispersion coefficients. This is mostly quenched in molecules by bond formation or electron transfer.

The DFT-D3 method can be coupled with any standard density functional, is applicable to all elements of the Periodic Table, to molecules and solids, and achieves (within about 10% tipically) Coupled Clusters considering single, double and triple excitations (CCSD(T)) accuracy [87]. This holds for vdW complexes as well as for intramolecular noncovalent interactions that very often occur in conformational problems. The method is furthermore robust, numerically stable, easily programmable, very fast, and allows for the straightforward computation of analytical gradients (forces). All necessary input parameters (cutoff radii and dispersion coefficients) are computed ab initio by Kohn-Sham DFT/time dependent DFT methods using extended AO basis sets close to the limit. The main conceptual advantage that is mostly responsible for the increased accuracy, is the use of structure dependent dispersion coefficients that are based on accurate first-principles (Time dependent DFT) calculations. One of the very big advantages of this method is that structural data are used but no atom connectivity information is required and

everything is computed only from Cartesian coordinates and atomic numbers. This method has been thoroughly tested not only on common organic, noncovalently bound complexes but also large, infinite, "heavy", and metalic systems have been considered [87]. In all cases tested, high accuracy has been obtained.

3 Results

In this chapter we show the results of the first-principles calculations of the electronic structure and atomic configuration of some biological molecules inside the BNNT using different approximations (Hartree-Fock, DFT, and DFT-D3). Also, a comparation of the energies obtained with the different approaches. The basis set superposition error was computed in the case of Hartree-Fock approximation. Finally, the density of states of the optimized configurations was calculated.

The nanotube considered is a zigzag (12,0) single-walled BNNT. The nanotube must be of finite length because of the cluster computer memory limitations, it consists of 12 planes of B and N plus 2 planes of hydrogens at the ends, giving a total of 168 atoms ($B_{72}N_{72}H_{24}$), as shown in Fig. 3.1. The size of the nanotube was chosen to be 14 planes because the energy change compared with 12 or 16 planes is negligible, and also the molecules were fitted in the center of the BNNT with negligible hydrogen contribution. The BNNT was saturated at the ends with hydrogen atoms to prevent the program breaks the nanotube when calculating the minimum energy structure, this is because when the program is relaxing the structure it seeks to saturate the B and N bonds.

The computational tool to carry out the calculations is a high performance cluster, which consists of 36 regular compute nodes (motherboard), each node contains 2 processors Intel® Xeon® six core X5670 2.93 GHz, 12MB Cache, 6.4 GT/s LGA 1366. The total memory per node is up to 48 GB Unbuffered DIMM.

All calculations were performed by employing the General Atomic and Molecular Electronic Structure System (GAMESS) [88]. The approximations used were Hartree-Fock, DFT, and DFT-D3 to take into account the dispersion interactions missing in standard DFT calculations [89]. The basis set used was a Gaussian basis (6-31G), and the functional used was B3LYP, which

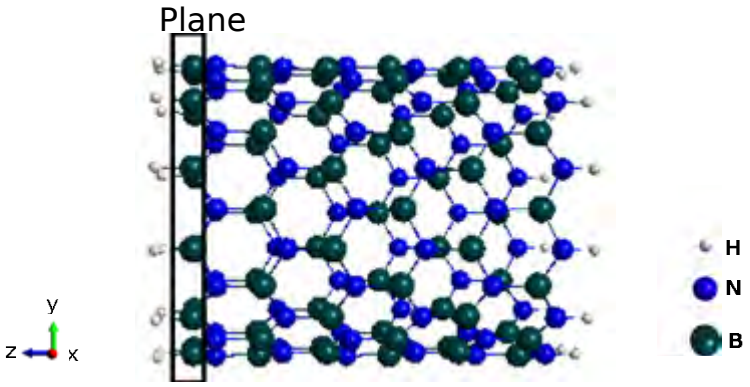

Figure 3.1: Zigzag (12,0) BNNT.

is a hybrid of exact (Hartree-Fock) exchange with local and gradient-corrected exchange and correlation terms, as first suggested by Becke [72]. The geometry optimization is the search for stationary points, which are places on the potential energy surface with a zero gradient vector (first derivative of the energy with respect to nuclear coordinates). These include minima (whether relative or global), as well as transition states (also known as saddle points). The two types of stationary points have a precise mathematical definition, depending on the curvature of the potential energy surface at these points. If all of the eigenvalues of the Hessian matrix (second derivative of the energy with respect to nuclear coordinates) are positive, the stationary point is a minimum. If there is one, and only one, negative curvature, the stationary point is a transition state. Points with more than one negative curvature do exist, but are not important in chemistry. Geometry searches are most effectively done by what is called a quasi-Newton-Raphson procedure. These methods assume a quadratic potential surface, and require the exact gradient vector and an approximation to the Hessian. It is the approximate nature of the Hessian that makes the method "quasi". The nature of convergence of the geometry search depends on how quadratic the real surface is, and the quality of the Hessian. GAMESS contains different implementations of quasi-Newton-Raphson procedures for finding stationary points: Newton-Raphson, Rational Function Optimization, Quadratic Approximation, and quasi-Newton-Raphson optimizer by Schlegel. They differ primarily in how the step size and direction are controlled, and how the Hessian is updated. The method used in this work was Quadratic Approximation, which is a version of an augmented Hessian technique. It employs Hessian shift parameter(s) in order to control the step length and direction. In this method the shift parameter is determined by

the requirement that the step size should equal 0.3 Bohr. There is only one shift parameter for both minima and transition states searches. The augmented Hessian will have the correct structure. There is another way of describing the same algorithm, namely as a minimization on the "image" potential. The latter is known as TRIM (Trust Radius Image Minimization). The Quadratic Approximation algorithm may be viewed as method for guiding the search in the "correct" direction when starting far from the stationary point. Once the stationary point is approached, the Quadratic Approximation method switches to Newton-Raphson, automatically, when the Newton-Raphson step-length drops below 0.1 or 0.3 Bohr, whichever is the smallest.

Although quasi-Newton-Raphson methods require only an approximation to the true Hessian, the quality of this matrix has a great affect on convergence of the geometry search. In this work was used a procedure contained within GAMESS for calculating a positive definite Hessian matrix. If Cartesian coordinates are used, the calculated Hessian is based on pairwise atom stretches. The calculation often works well for minima, but cannot possibly find transition states (because it is positive definite). Calculating the Hessian matrix may lead to significantly more steps in the geometry search.

Taking into account the previous specifications, the convergence of SCF is achieved when the density change between two consecutive SCF cycles is less than 1.0×10^{-5} in absolute value. Geometry searches do not bring the gradient exactly to zero. Instead they stop when the largest component of the gradient vector is below the value of 2.0×10^{-4} (Hartree/Bohr), and the root mean square (RMS) gradient vector less than $\frac{2}{3}\times10^{-4}$.

After the optimization of the BNNT, the N atoms were moved slightly outward and the B atoms were moved slightly inward from the tube center, which is consistent with the previous ab initio calculations on BNNT geometries [14, 90].

The length of translational vector, average diameter and B-N bond length in the optimized configuration of the BNNT for each approximation is shown in table 3.1.

The length of translational vector matches the previously reported first-principles calculation [91]. The values of the B-N bond length are consistent with previously reported DFT calculations [92], and also are in good agreement with the experimental value of 1.45 Å [93].

Table 3.1: Translational vector, diameter and B-N bond length of the optimized BNNT.

	Hartree-Fock (Å)	DFT (Å)	DFT-D3 (Å)
Translational vector	4.33	4.36	4.36
BNNT diameter	9.79	9.81	9.80
B-N bond length	1.448	1.45	1.45

The geometry-optimized structures for the BNNTs at each level of theory give an energy that corresponds to that of equilibrium or ground-state energy. Table 3.2 shows the ground-state energies obtained in Hartree and eV units (1 Hartree=27.2113 eV).

Table 3.2: Ground-state energy of the optimized pristine BNNT.

	Hartree-Fock		DFT		DFT-D3	
	Hartree	keV	Hartree	keV	Hartree	keV
Ground-state energy	-5718.589	-155.610	-5749.531	-156.452	-5749.830	-156.460

The organic molecules considered in this work are three amino acids and five nitrogenous bases: glycine, serine, cysteine, cytosine, thymine, uracil, adenine and guanine. The optimized structure of each molecule was calculated, and is shown in Fig. 3.2 along with their corresponding molecular formula.

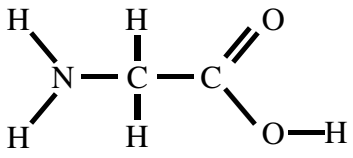

$C_2H_5NO_2$

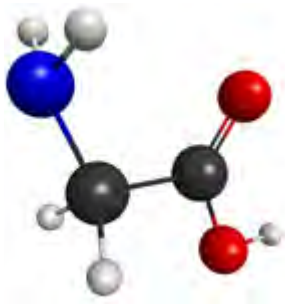

(a)

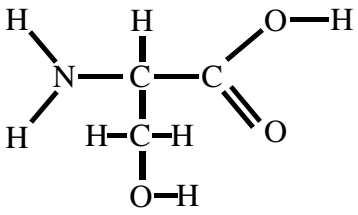

$C_3H_7NO_3$

(b)

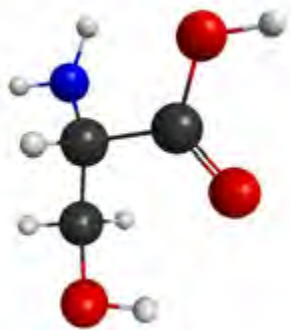

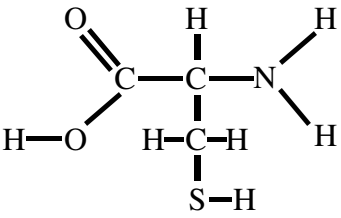

$C_3H_7NO_2S$

(c)

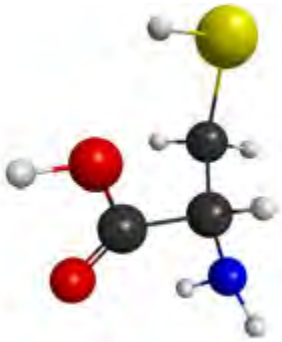

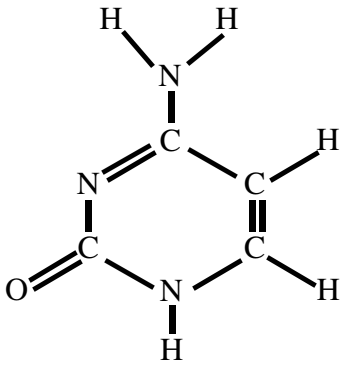

$C_4H_5N_3O$

(d)

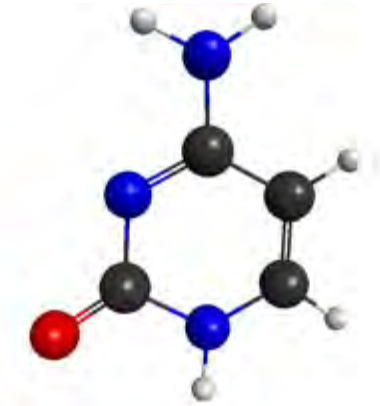

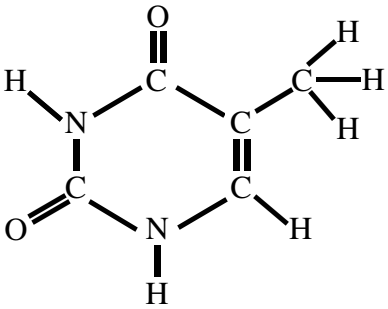

$C_5H_6N_2O_2$

(e)

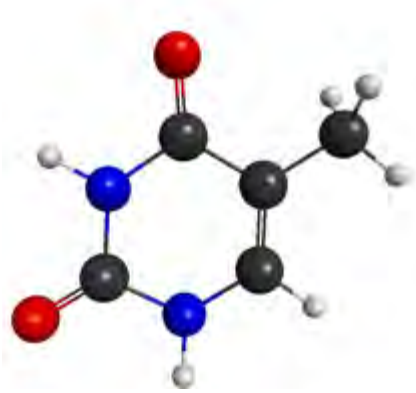

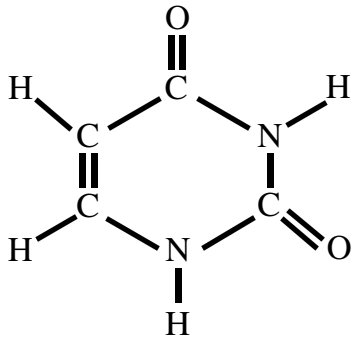

$C_4H_4N_2O_2$

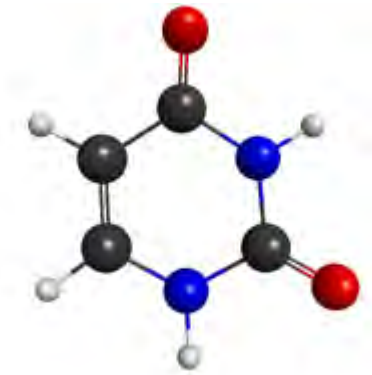

(f)

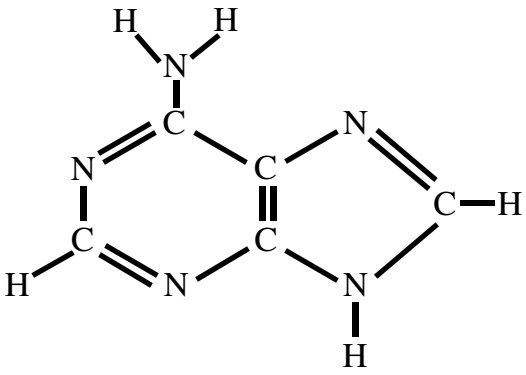

$C_5H_5N_5$

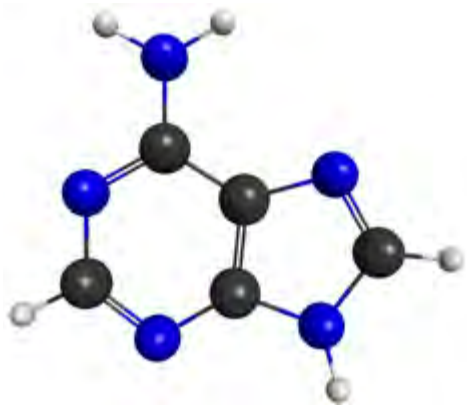

(g)

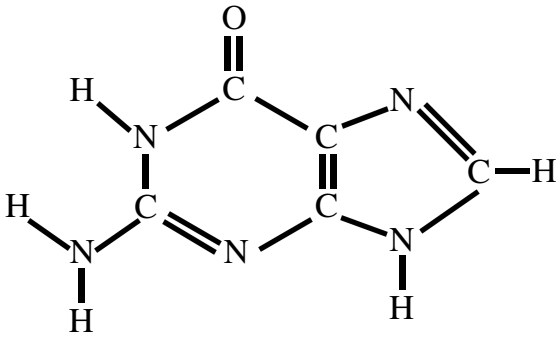

$C_5H_5N_5O$

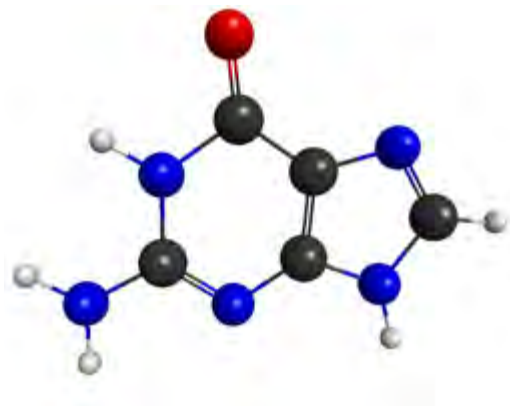

(h)

Figure 3.2: Equilibrium geometry of (a) glycine, (b) serine, (c) cysteine, (d) cytosine, (e) thymine, (f) uracil, (g) adenine and (h) guanine.

The ground-state energies of each optimized structures of the organic molecules at each level of theory are shown in table 3.3.

Table 3.3: Ground-state energies of the optimized organic molecules.

	Hartree-Fock		DFT		DFT-D3	
	Hartree	keV	Hartree	keV	Hartree	keV
Glycine	-282.698	-7.692	-284.179	-7.732	-284.184	-7.733
Serine	-396.536	-10.790	-398.606	-10.846	-398.617	-10.846
Cysteine	-719.184	-19.569	-721.546	-19.634	-721.558	-19.634
Cytosine	-392.437	-10.678	-394.591	-10.737	-394.598	-10.737
Thymine	-451.304	-12.280	-453.753	-12.347	-453.763	-12.347
Uracil	-412.280	-11.218	-414.471	-11.278	-414.478	-11.278
Adenine	-464.296	-12.634	-466.900	-12.704	-466.909	-12.705
Guanine	-539.138	-14.670	-542.079	-14.750	-542.090	-14.751

Once the equilibrium geometries of the BNNT and the organic molecules were found, each molecule was placed inside the BNNT and each structure was optimized using the same approximations described above. Fig. 3.3 shows the equilibrium geometries obtained.

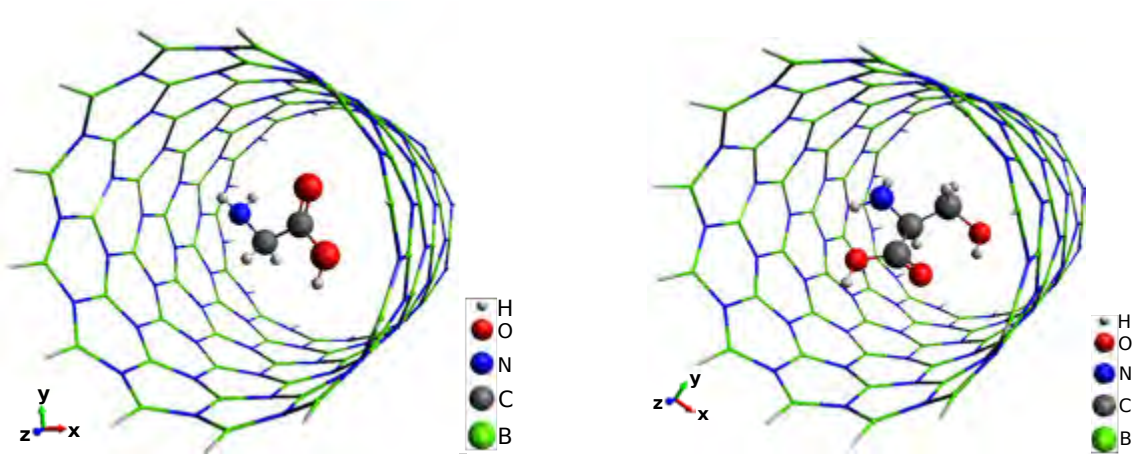

(a) (b)

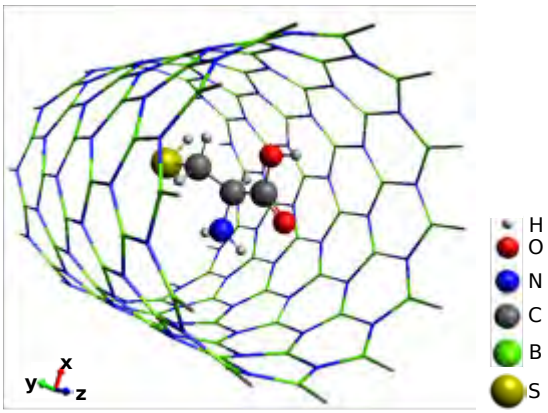

(c)

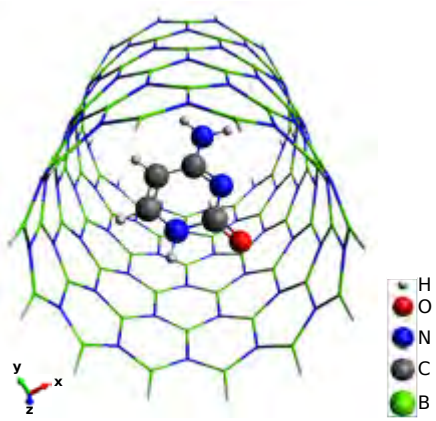

(d)

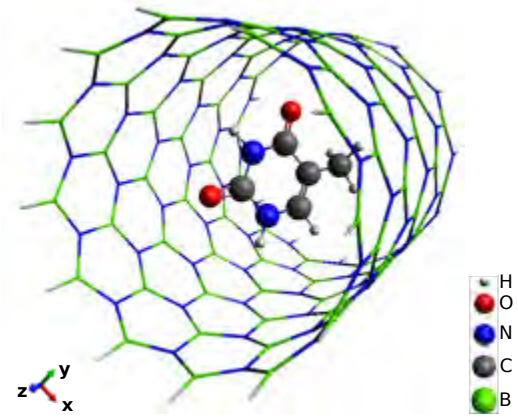

(e)

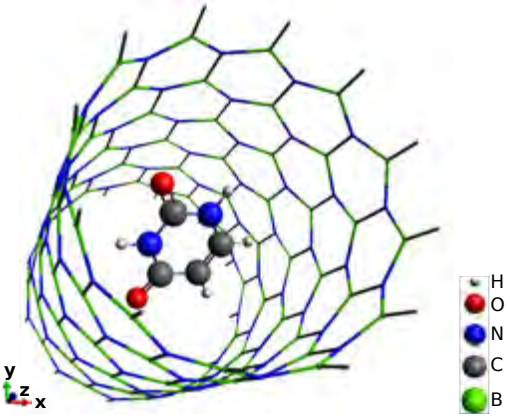

(f)

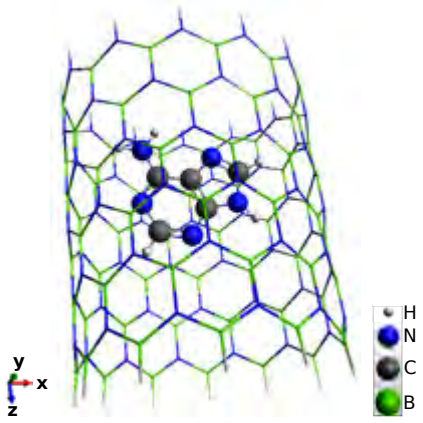

(g)

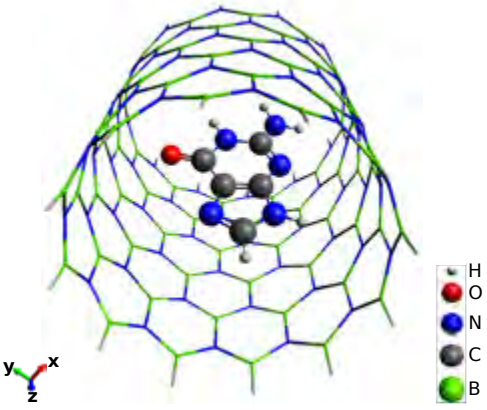

(h)

Figure 3.3: Equilibrium geometry of a zigzag (12,0) BNNT encapsulating (a) glycine, (b) serine, (c) cysteine, (d) cytosine, (e) thymine, (f) uracil, (g) adenine and (h) guanine.

The optimization process not only forces the molecule to reposition itself but can distort the BNNT in the case of large molecules.

The nearest distance between the center of mass of each molecule and the BNNT was measured and the results are in table 3.4.

Table 3.4: Nearest distance between the center of mass of the molecule and the BNNT.

	Hartree-Fock (Å)	DFT (Å)	DFT-D3 (Å)
Glycine	4.58	4.56	4.54
Serine	4.22	4.30	4.15
Cysteine	4.52	4.47	4.15
Cytosine	4.36	4.42	4.37
Thymine	4.33	4.22	4.22
Uracil	4.34	4.23	4.39
Adenine	4.32	4.39	4.30
Guanine	4.47	4.53	4.42

The ground-state energies of the optimized structures of the BNNT encapsulating the organic molecules at each level of theory are shown in table 3.5.

Table 3.5: Ground-state energies of the equilibrium geometries of BNNT encapsulating the organic molecules.

BNNT	Hartree-Fock		DFT		DFT-D3	
encapsulating:	Hartree	keV	Hartree	keV	Hartree	keV
Glycine	-6001.294	-163.303	-6033.721	-164.185	-6034.062	-164.195
Serine	-6115.133	-166.401	-6148.149	-167.299	-6148.510	-167.309
Cysteine	-6437.781	-175.180	-6471.087	-176.087	-6471.455	-176.097
Cytosine	-6111.039	-166.289	-6144.136	-167.190	-6144.494	-167.200
Thymine	-6169.900	-167.891	-6203.293	-168.800	-6203.663	-168.810
Uracil	-6130.876	-166.829	-6164.012	-167.731	-6164.371	-167.741
Adenine	-6182.864	-168.244	-6216.418	-169.157	-6216.794	-169.167
Guanine	-6257.733	-170.281	-6291.621	-171.203	-6291.997	-171.213

Once the total energies of the isolated BNNT, the organic molecules and the combined structures were obtained, it is possible to calculate the binding energy for the interacting system by

$$E_b = E_{BNNT+m} - E_m - E_{BNNT}, \tag{3.1}$$

where E_{BNNT+m} is the energy of the BNNT encapsulating the organic molecule, E_m is the energy of the molecule, and E_{BNNT} is the energy of the BNNT. Table 3.6 shows the binding energies obtained at each level of theory.

Table 3.6: Binding energies of the BNNT encapsulating the organic molecules.

BNNT	Hartree-Fock		DFT		DFT-D3	
encapsulating:	Hartree	eV	Hartree	eV	Hartree	eV
Glycine	-0.007	-0.205	-0.010	-0.280	-0.048	-1.297
Serine	-0.008	-0.224	-0.011	-0.311	-0.063	-1.706
Cysteine	-0.008	-0.215	-0.010	-0.276	-0.066	-1.808
Cytosine	-0.013	-0.353	-0.015	-0.398	-0.066	-1.801
Thymine	-0.007	-0.182	-0.009	-0.265	-0.070	-1.913
Uracil	-0.007	-0.203	-0.010	-0.274	-0.063	-1.706
Adenine	0.020	0.553	0.013	0.359	-0.055	-1.499
Guanine	-0.006	-0.170	-0.011	-0.297	-0.077	-2.090

In the previous calculations, the energy of the fragments (BNNT and organic molecules) was calculated with the basis functions associated with the atoms only in that fragment. However, the energy of the whole system uses the basis functions of both fragments. Therefore, there is a systematic error in the interaction energies because the energy of each one of the fragments calculated using the full basis, which is consistent with that of the whole system, is lower than the one calculated with only its own basis set. The result is that the interaction energies are overestimated [64].

An approximate way of correcting this problem is to calculate the energy of the fragments using augmented basis, i.e. its own basis functions together with those of the other fragment (ghost orbitals) [94]. This is known as *counterpoise correction*. In the limit of a complete basis set the counterpoise correction vanishes, but for truncated basis sets the effect may be quite

important, especially for weakly bound systems such as van der Waals complexes. Since basis sets used in practice are of finite size, at nuclear configurations where the two fragments are in proximity (i.e. at the equilibrium geometry of the complex BNNT+molecule), the basis functions centered on the BNNT assist in lowering the energy of the molecule and vice versa, an effect first named *basis set superposition error* (BSSE) [95].

If the correction is estimated using the counterpoise correction, then it will not converge to the same result at the complete basis set limit since the reference energies of BNNT and the molecules are evaluated at different geometries (complex vs isolated). This problem can be overcome by estimating the BSSE by

$$\begin{aligned} E_{BSSE} &= E^{\alpha\cup\beta}_{BNNT,m}(BNNT,m) - E^{\alpha\cup\beta}_{BNNT,m}(BNNT) - E^{\alpha\cup\beta}_{BNNT,m}(m) \\ &\quad + E^{\alpha}_{rel}(BNNT) + E^{\beta}_{rel}(m), \end{aligned} \tag{3.2}$$

where $\alpha \cup \beta$ is the complex basis set, $E^{\alpha}_{rel}(BNNT) = E^{\alpha}_{BNNT.m}(BNNT) - E^{\alpha}_{BNNT}(BNNT)$ and $E^{\beta}_{rel}(m) = E^{\beta}_{BNNT.m}(m) - E^{\beta}_{m}(m)$ are the fragment relaxation energies corresponding to the energy penalty for distorting them from their isolated geometries to the ones in the complex [96].

Since $E^{\alpha}_{rel}(BNNT)$ and $E^{\beta}_{rel}(m)$ are small for most weakly bound complexes, they are often omitted from the evaluation of the BSSE-corrected interaction energy. However, in this work the BSSE was calculated using Eq. (3.2) in the case of Hartree-Fock approximation, and the results are shown in table 3.7.

Table 3.7: BSSE-corrected binding energies in Hartree-Fock approximation.

BNNT encapsulating:	E_{BSSE} (eV)	E_b (eV)
Glycine	0.086	-0.291
Serine	0.197	-0.421
Cysteine	0.134	-0.349
Cytosine	0.010	-0.363
Thymine	0.211	-0.393
Uracil	0.134	-0.336
Adenine	1.048	-0.495
Guanine	0.333	-0.503

From the results in table 3.6 and the BSSE-corrected energies for Hartree-Fock in table 3.7 it can be seen that the adsorption magnitude exhibits the following order Cytosine > Serine > Cysteine > Glycine ≈ Uracil > Thymine > Guanine > Adenine for the Hartree-Fock approximation; Guanine > Adenine > Serine > Thymine > Cytosine > Cysteine > Uracil > Glycine for the BSSE-corrected Hartree-Fock approximation; Cytosine > Serine > Guanine > Glycine > Cysteine ≈ Uracil > Thymine > Adenine for the DFT approximation; Guanine > Thymine > Cysteine ≈ Cytosine > Serine = Uracil > Adenine > Glycine for the DFT-D3 approximation. It can be noticed that Cytosine is the most adsorbed molecule and Adenine is the less adsorbed molecule in the case of Hartree-Fock and DFT approximations, while Guanine is the most adsorbed molecule and Glycine is the less adsorbed molecule in the case of BSSE-corrected Hartree-Fock and DFT-D3 approximations. This can be explained from the fact that in Hartree-Fock are obtained the classic electrostatic energy (the Hartree term) and the exchange energy, while in DFT approximation are obtained the electrostatic energy, the exchange energy and the correlation energy, which is the smallest contribution to the total interaction energy. In the case of BSSE-corrected Hartree-Fock is taken into account the error of considering a non complete basis set, and in DFT-D3 approximation is taken into account the dispersion interactions missing in DFT calculations.

An important fact in the optimization process is that adenine remains in the center of the BNNT while the others molecules exhibit more movement and the oxygen atoms tend to approach to the inner surface of the nanotube. This can be explained from the fact that the partially negatively charged oxygen atom can interact electrostatically with the polar network of the heteronucleic BNNT inner surface, specifically in an attractive manner with the partial positive charges on boron, and repulsively with the partial negative charges on nitrogen.

The results in table 3.6 and table 3.7 show that there is physisorption, i.e., adsorption in which the forces involved are intermolecular forces (van der Waals forces) and which do not involve a significant change in the electronic orbital patterns of the species involved. To see if the perturbation of the electronic states of adsorbent and adsorbate is minimal, the electronic density of states (DOS) was calculated for the optimized structures, as shown in Fig. 3.4.

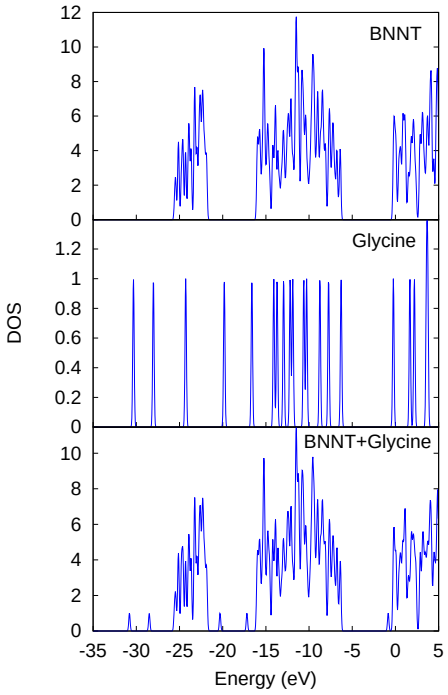
BNNT
Glycine
BNNT+Glycine
DOS
Energy (eV)

(a)

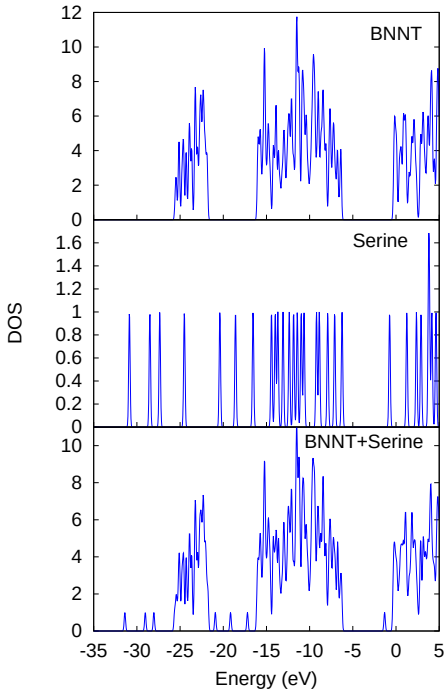
BNNT
Serine
BNNT+Serine
DOS
Energy (eV)

(b)

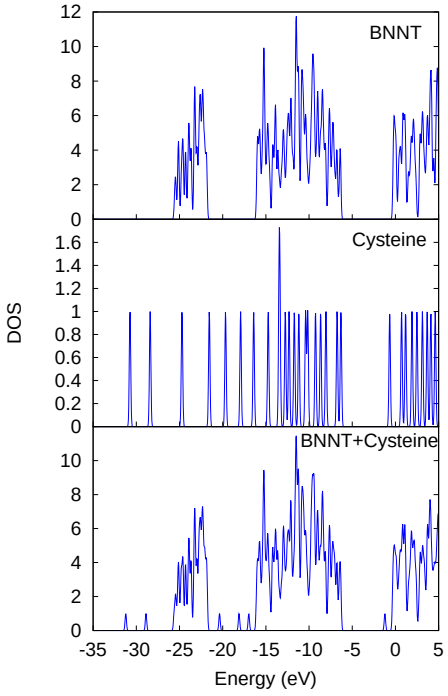
BNNT
Cysteine
BNNT+Cysteine
DOS
Energy (eV)

(c)

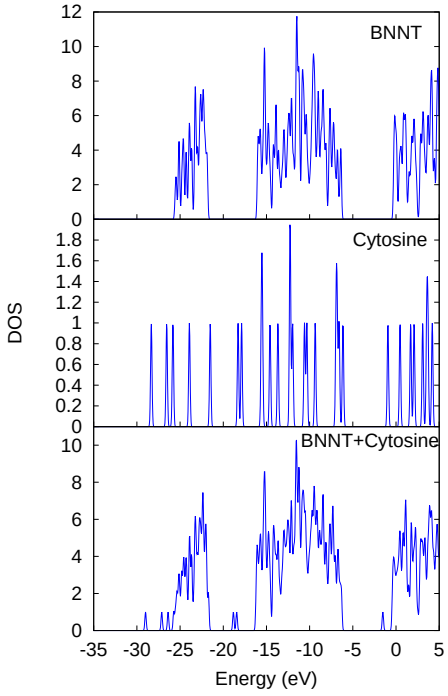
BNNT
Cytosine
BNNT+Cytosine
DOS
Energy (eV)

(d)

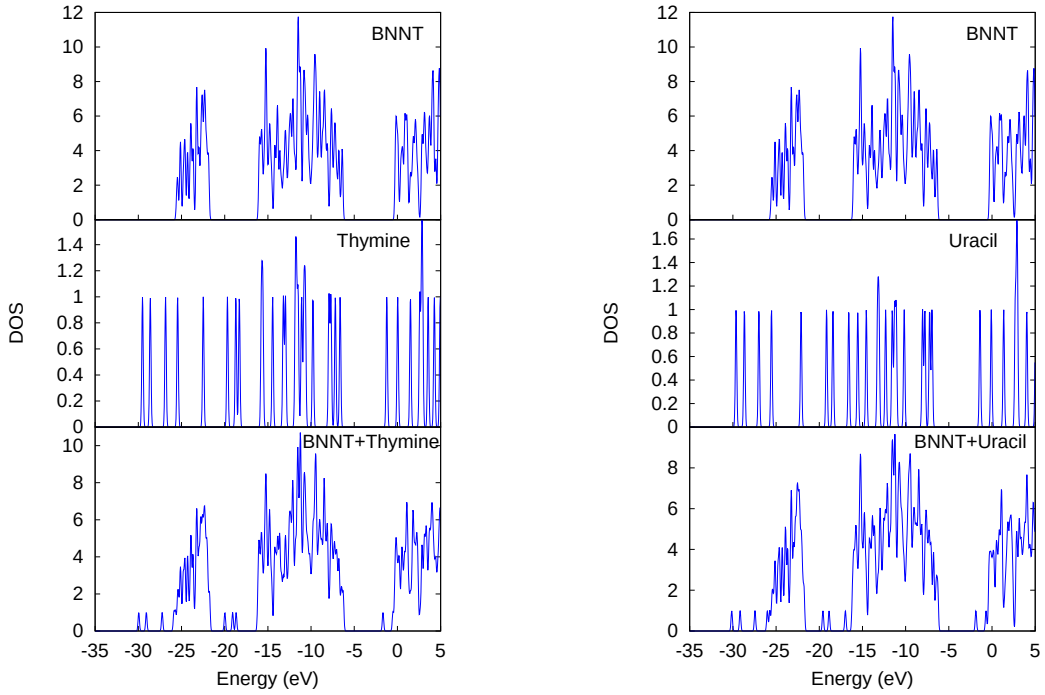

(e)

(f)

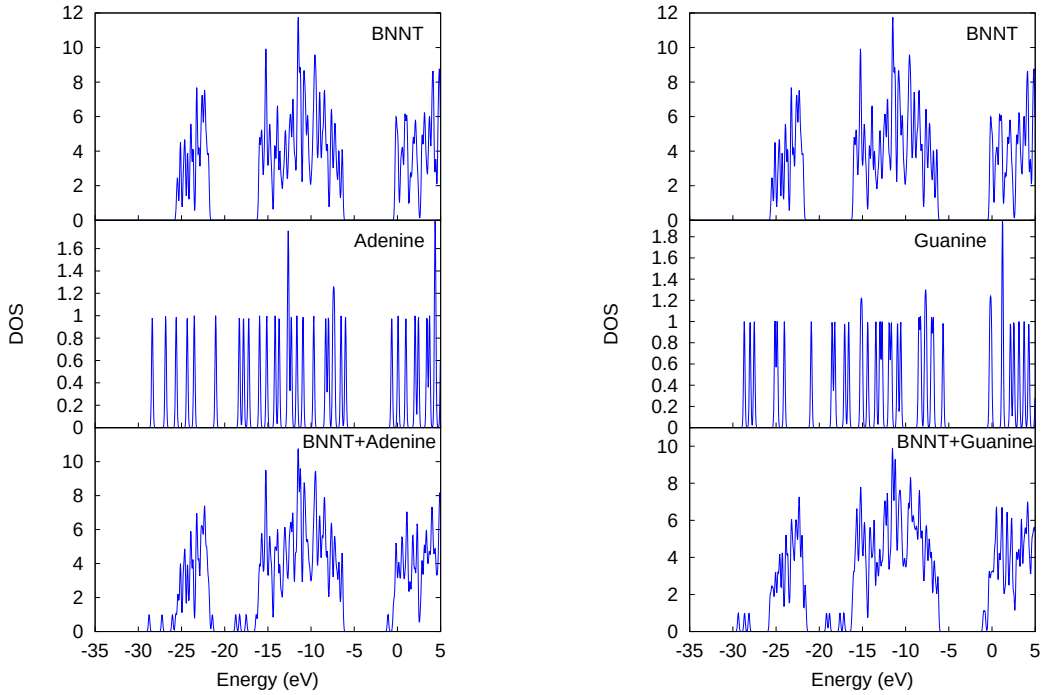

(g)

(h)

Figure 3.4: Density of states of the equilibrium geometry of a zigzag (12,0) BNNT encapsulating (a) glycine, (b) serine, (c) cysteine, (d) cytosine, (e) thymine, (f) uracil, (g) adenine and (h) guanine. Top panel: pristine zigzag (12,0) BNNT, middle panel: isolated molecule, and bottom panel: BNNT encapsulating the molecule.

In the calculated DOS, the bottom panel seems to be the sum of the top and middle panels with a slight shift of energy levels of the molecule, and some scaling in the height of DOS. The appearance of the mid-gap states in the bottom panel represents a mixing of electronic states of the molecules and the BNNT. It may be noted that the shift of energy levels in the case of BNNT encapsulating adenine is negligible, this can be due to adenine does not have an oxygen atom and there is a very small charge transfer from the BNNT to oxygen in molecules (except adenine) and may indicate the presence of a relatively weaker electrostatic interaction between the BNNT and the molecules. However, the interaction between BNNT and the organic molecules is essentially dominated by the vdW forces.

The band gap of the pristine BNNT is 5.24 eV, which is in agreement with previously reported band gap of BNNTs between 5.0-6.0 eV [1]. The band gap correspondent to the BNNT encapsulating the organic molecules is shown in table 3.8.

Table 3.8: Band gap of BNNT encapsulating the organic molecules.

BNNT encapsulating:	Band gap (eV)
Glycine	5.40
Serine	5.24
Cysteine	5.28
Cytosine	5.20
Thymine	5.04
Uracil	4.88
Adenine	5.20
Guanine	5.28

The changes in the band gap values are due to there is a very small hybridization of orbitals from the molecules and those from the nanotube. However, the BNNT shows a chemically inert behavior.

The previous results show that regardless of the final configuration the encapsulation assumes, there is no chemical adsorption between the organic molecules and the BNNT, under the different approximations.

4 Conclusions

Theoretical studies along with computational resources, constitute a very powerful tool that allows to observe, measure and even predict the molecular interaction of any desired structure with a high precision. In this thesis we studied theoretically the interactions between some organic molecules inside a BNNT by using different approximations like Hartree-Fock, DFT, and DFT-D3, and we compared the binding energy of each method.

The organic molecules studied were three amino acids (glycine, serine, cysteine) and five nitrogenous bases (cytosine, thymine, uracil, adenine, guanine). We chose these molecules because amino acids play central roles both as building blocks of proteins and as intermediates in metabolism, and the nitrogenous bases are used in the construction of nucleotides, which in turn build up the nucleic acids like DNA and RNA. These molecules were placed inside a BNNT, because this nanotube presents attractive properties including chemical inertness.

The results of the optimized BNNT for all the approximations are in agreement with previously reported DFT calculations and experimental values. This indicate that the B3LYP functional used is a good choice for this type of structure.

The optimized structures of the organic molecules inside the BNNT show that the molecules are practically in the center of the nanotube, with only a slight atraction of the oxygen atoms to boron atoms, because of the electrostatically interaction with the polar network of the heteronucleic BNNT inner surface.

Although there are no experimental values to compare the theoretical results, the binding energies obtained for each approximation (including the BSSE-corrected binding energies in Hartree-Fock approximation) show that there is physisorption. This was confirmed by the calculated DOS, which do not show a significant change in the electronic states of the BNNT and the

organic molecule. These results also indicate that the interaction between the BNNT and the molecules is dominated by the vdW forces. These results indicate that the BNNTs can be used as a tool for transporting organic molecules inside a cavity.

As future work, more first-principles calculations of similar structures can be done, for example, using a BNNT with a bigger diameter. Also, using a hybrid structure of BNNT with carbon atoms. These works are intended to study the possibility of constructing biosensors and using the nanotubes as a tool to deliver drug to specific cells as part of the future medicine.

References

[1] C. Zhi, Y. Bando, C. Tang, D. Golberg. *Boron nitride nanotubes*. Mater. Sci. Eng. R **70**, 92-111, (2010)

[2] A. Rubio, J. L. Corkill, M. L. Cohen. *Theory of graphitic boron nitride nanotubes*. Phys. Rev. B **49**, 5081-5084, (1994)

[3] X. Blase, A. Rubio, S. G. Louie, M. L. Cohen. *Stability and Band Gap Constancy of Boron Nitride Nanotubes*. Europhys. Lett. **28**, 335, (1994)

[4] N. G. Chopra, R. J. Luyken, K. Cherrey, V. H. Crespi, M. L. Cohen, S. G. Louie, A. Zettl. *Boron Nitride Nanotubes*. Science **269**, 966-967, (1995)

[5] H. J. Xiang, J. Yang, J. G. Hou, Q. Zhu. *First-principles study of small-radius single-walled BN nanotubes*. Phys. Rev. B **68**, 35427, (2003)

[6] Y. Miyamoto, A. Rubio, M. L. Cohen, S. G. Louie. *Chiral tubules of hexagonal BC_2N*. Phys. Rev. B **50**, 4976-4979, (1994)

[7] Y.-H. Kim, K. J. Chang, S. G. Louie. *Electronic structure of radially deformed BN and BC_3 nanotubes*. Phys. Rev. B **63**, 205408, (2001)

[8] K. H. Khoo, M. S. C. Mazzoni, S. G. Louie. *Tuning the electronic properties of boron nitride nanotubes with transverse electric fields: A giant dc Stark effect*. Phys. Rev. B **69**, 201401(R), (2004)

[9] C.-W. Chen, M.-H. Lee, S. J. Clark. *Band gap modification of single-walled carbon nanotube and boron nitride nanotube under a transverse electric field*. Nanotechnology **15**, 1837, (2004)

[10] M. Ishigami, J. D. Sau, S. Aloni, M. L. Cohen, A. Zettl. *Observation of the Giant Stark Effect in Boron-Nitride Nanotubes*. Phys. Rev. Lett. **94**, 056804, (2005)

[11] E. Hernandez, C. Goze, P. Bernier, A. Rubio. *Elastic Properties of C and $B_xC_yN_z$ Composite Nanotubes*. Phys. Rev. Lett. **80**, 4502-4505, (1998)

[12] R. Arenal, M.-S. Wang, Z. Xu, A. Loiseau, D. Golberg. *Young modulus, mechanical and electrical properties of isolated individual and bundled single-walled boron nitride nanotubes*. Nanotechnology **22**, 265704, (2011)

[13] D. Sánchez-Portal, E. Hernández. *Vibrational properties of single-wall nanotubes and monolayers of hexagonal BN*. Phys. Rev. B **66**, 235415, (2002)

[14] L. Wirtz, A. Rubio, R. A. de la Concha, A. Loiseau. *Ab initio calculations of the lattice dynamics of boron nitride nanotubes*. Phys. Rev. B **68**, 045425, (2003)

[15] V. N. Popov. *Lattice dynamics of single-walled boron nitride nanotubes*. Phys. Rev. B **67**, 085408, (2003)

[16] Y. Xiao, X. H. Yan, J. X. Cao, J. W. Ding, Y. L. Mao, J. Xiang. *Specific heat and quantized thermal conductance of single-walled boron nitride nanotubes*. Phys. Rev. B **69**, 205415, (2004)

[17] C. Tang, Y. Bando, C. Liu, S. Fan, J. Zhang, X. Ding, D. Golberg. *Thermal Conductivity of Nanostructured Boron Nitride Materials*. J. Phys. Chem. B **110**, 10354-10357, (2006)

[18] Y. Chen, J. Zou, S. J. Campbell, G. Le Caer. *Boron nitride nanotubes: Pronounced resistance to oxidation*. Appl. Phys. Lett. **84**, 2430, (2004)

[19] A. Zettl, C. W. Chang, G. Begtrup. *A new look at thermal properties of nanotubes*. Physica Status Solidi B **244**, 4181-4183, (2007)

[20] C. W. Chang, D. Okawa, H. Garcia, A. Majumdar, A. Zettl. *Breakdown of Fourier's Law in Nanotube Thermal Conductors*. Phys. Rev. Lett. **101**, 075903, (2008)

[21] I. Savic, D. A. Stewart, N. Mingo. *Thermal conduction mechanisms in boron nitride nanotubes: Few-shell versus all-shell conduction*. Phys. Rev. B **78**, 235434, (2008)

[22] C. W. Chang, W.-Q. Han, A. Zettl. *Thermal conductivity of B-C-N and BN nanotubes*. J. Vac. Sci. Technol. B **23**, 1883, (2005)

[23] M.-F. Ng and R. Q. Zhang. *Optical spectra of single-walled boron nitride nanotubes*. Phys. Rev. B **69**, 115417, (2004)

[24] P. Kral, E. J. Mele, D. Tomanek. *Photogalvanic Effects in Heteropolar Nanotubes*. Phys. Rev. Lett. **85**, 1512-1515, (2000)

[25] J. Kongsted, A. Osted, L. Jensen, P.-O. Astrand, K. V. Mikkelsen. *Frequency-Dependent Polarizability of Boron Nitride Nanotubes: A Theoretical Study*. J. Phys. Chem. B **105**, 10243-10248, (2001)

[26] A. Loiseau, F. Willaime, N. Demoncy, G. Hug, H. Pascard. *Boron Nitride Nanotubes with Reduced Numbers of Layers Synthesized by Arc Discharge*. Phys. Rev. Lett. **76**, 4737-4740, (1996)

[27] A. Loiseau, F. Willaime, N. Demoncy, N. Schramchenko, G. Hug, C. Colliex, H. Pascard. *Boron nitride nanotubes*. Carbon **36**, 743-752, (1998)

[28] J. Cumings, A. Zettl. *Mass-production of boron nitride double-wall nanotubes and nanococoons*. Chem. Phys. Lett. **316**, 211-216, (2000)

[29] J. Wang, C. H. Lee, Y. Bando, D. Golberg, Y. K. Yap. *Multiwalled Boron Nitride Nanotubes: Growth, Properties, and Applications*. B-C-N Nanotubes and Related Nanostructures, Lecture Notes in Nanoscale Science and Technology **6**, 23-44, (2009)

[30] Y. Chen, L. T. Chadderton, J. Fitz Gerald, J. S. Williams. *A solid-state process for formation of boron nitride nanotubes*. Appl. Phys. Lett. **74**, 2960, (1999)

[31] S. Y. Bae, H. W. Seo, J. Park, Y. S. Choi, J. C. Park, S. Y. Lee. *Boron nitride nanotubes synthesized in the temperature range 1000-1200 °C*. Chem. Phys. Lett. **374**, 534-541, (2003)

[32] J. Yu, Y. Chen, R. Wuhrer, Z. Liu, S. P. Ringer. *In Situ Formation of BN Nanotubes during Nitriding Reactions*. Chem. Mater. **17**, 5172-5176, (2005)

[33] Y. Chen, M. Conway, J. S. Williams, J. Zou. *Large-quantity production of high-yield boron nitride nanotubes*. J. Mater. Res. **17**, 1896-1899, (2002)

[34] H. Chen, Y. Chen, Y. Liu, L. Fu, C. Huang, D. Llewellyn. *Over 1.0 mm-long boron nitride nanotubes*. Chem. Phys. Lett. **463**, 130-133, (2008)

[35] Y. Chen, J. Fitz Gerald, J. S. Williams, S. Bulcock. *Synthesis of boron nitride nanotubes at low temperatures using reactive ball milling*. Chem. Phys. Lett. **299**, 260-264, (1999)

[36] O. R. Lourie, C. R. Jones, B. M. Bartlett, P. C. Gibbons, R. S. Ruoff, W. E. Buhro. *CVD Growth of Boron Nitride Nanotubes*. Chem. Mater. **12**, 1808-1810, (2000)

[37] J. Wang, V. K. Kayastha, Y. K. Yap, Z. Fan, J. G. Lu, Z. Pan, I. N. Ivanov, A. A. Puretzky, D. B. Geohegan. *Low Temperature Growth of Boron Nitride Nanotubes on Substrates*. Nano Lett. **5**, 2528-2532, (2005)

[38] C. Tang, Y. Bando, T. Sato, K. Kurashima. *A novel precursor for synthesis of pure boron nitride nanotubes*. Chem. Commun., 1290-1291, (2002)

[39] C. C. Tang, X. X. Ding, X. T. Huang, Z. W. Gan, S. R. Qi, W. Liu, S. S. Fan. *Effective growth of boron nitride nanotubes*. Chem. Phys. Lett. **356**, 254-258, (2002)

[40] C. Zhi, Y. Bando, C. Tan, D. Golberg. *Effective precursor for high yield synthesis of pure BN nanotubes*. Solid State Commun. **135**, 67-70, (2005)

[41] M. J. Kim, S. Chatterjee, S. M. Kim, E. A. Stach, M. G. Bradley, M. J. Pender, L. G. Sneddon, B. Maruyama. *Double-Walled Boron Nitride Nanotubes Grown by Floating Catalyst Chemical Vapor Deposition*. Nano Lett. **8**, 3298-3302, (2008)

[42] G. Ciofani, V. Raffa, A. Menciassi, A. Cuschieri. *Cytocompatibility, interactions, and uptake of polyethyleneimine-coated boron nitride nanotubes by living cells: Confirmation of their potential for biomedical applications*. Biotechnology and Bioengineering **101**, 850-858, (2008)

[43] G. Ciofani, V. Raffa, A. Menciassi, P. Dario. *Preparation of Boron Nitride Nanotubes Aqueous Dispersions for Biological Applications*. J. Nanosci. Nanotechnol. **8**, 6223-6231, (2008)

[44] G. Ciofani, V. Raffa, A. Menciassi, A. Cuschieri. *Folate Functionalized Boron Nitride Nanotubes and their Selective Uptake by Glioblastoma Multiforme Cells: Implications for their Use as Boron Carriers in Clinical Boron Neutron Capture Therapy*. Nano. Res. Lett. **4**, 113-121, (2008)

[45] G. Ciofani, V. Raffa, A. Menciassi, A. Cuschieri. *Boron nitride nanotubes: An innovative tool for nanomedicine*. Nano Today **4**, 8-10, (2009)

[46] G. Ciofani, V. Raffa, J. Yu, Y. Chen, Y. Obata, S. Takeoka, A. Menciassi, A. Cuschieri. *Boron Nitride Nanotubes: A Novel Vector for Targeted Magnetic Drug Delivery*. Curr. Nanosci. **5**, 33-38, (2009)

[47] X. Chen, P. Wu, M. Rousseas, D. Okawa, Z. Gartner, A. Zettl, C. R. Bertozzi. *Boron Nitride Nanotubes Are Noncytotoxic and Can Be Functionalized for Interaction with Proteins and Cells*. J. Am. Chem. Soc. **131**, 890-891, (2009)

[48] G. Ciofani, S. Danti, G. G. Genchi, B. Mazzolai, V. Mattoli. *Boron Nitride Nanotubes: Biocompatibility and Potential Spill-Over in Nanomedicine*. Small **9**, 1672-1685, (2013)

[49] G. Ciofani, S. Danti, S. Nitti, B. Mazzolai, V. Mattoli, M. Giorgi. *Biocompatibility of boron nitride nanotubes: An up-date of in vivo toxicological investigation*. Int. J. Pharm. **444**, 85-88, (2013)

[50] Z. Zhou, J. Zhao, Z. Chen, X. Gao, T. Yan, B. Wen, P. V. R. Schleyer. *Comparative Study of Hydrogen Adsorption on Carbon and BN Nanotubes*. J. Phys. Chem. B **110**, 13363-13369, (2006)

[51] G. Mpourmpakis, G. E. Froudakis. *Why boron nitride nanotubes are preferable to carbon nanotubes for hydrogen storage?: An ab initio theoretical study*. Catalysis Today **120**, 341-345, (2007)

[52] X. Wu, J. L. Yang, X. C. Zeng. *Adsorption of hydrogen molecules on the platinum-doped boron nitride nanotubes*. J. Chem. Phys. **125**, 044704, (2006)

[53] R. J. Baierle, P. Piquini, T. M. Schmidt, A. Fazzio. *Hydrogen Adsorption on Carbon-Doped Boron Nitride Nanotube*. J. Phys. Chem. B **110**, 21184-21188, (2006)

[54] R. Ma, Y. Bando, H. Zhu, T. Sato, C. Xu, D. Wu. *Hydrogen Uptake in Boron Nitride Nanotubes at Room Temperature*. J. Am. Chem. Soc. **124**, 7672-7673, (2002)

[55] X. Chen, X. P. Gao, H. Zhang, Z. Zhou, W. K. Hu, G. L. Pan, H. Y. Zhu, T. Y. Yan, D. Y. Song. *Preparation and Electrochemical Hydrogen Storage of Boron Nitride Nanotubes*. J. Phys. Chem. B **109**, 11525-11529, (2005)

[56] T. A. Hilder, D. Gordon, S.-H. Chung. *Salt Rejection and Water Transport Through Boron Nitride Nanotubes*. Small **5**, 2183-2190, (2009)

[57] J. Ravichandran, A. G. Manoj, J. Liu, I. Manna, D. L. Carroll. *A novel polymer nanotube composite for photovoltaic packaging applications*. Nanotechnology **19**, 085712, (2008)

[58] N. P. Bansal, J. B. Hurst, S. R. Choi. *Boron Nitride Nanotubes-Reinforced Glass Composites*. Journal of the American Ceramic Society **89**, 388-390, (2006)

[59] Q. Huang, Y. Bando, X. Xu, T. Nishimura, C. Zhi, C. Tang, F. Xu, L. Gao, D. Golberg. *Enhancing superplasticity of engineering ceramics by introducing BN nanotubes*. Nanotechnology **18**, 485706, (2007)

[60] M. Yamaguchi, A. Pakdel, C. Zhi, Y. Bando, D.-M. Tang, K. Faerstein, D. Shtansky, D. Golberg. *Utilization of multiwalled boron nitride nanotubes for the reinforcement of lightweight aluminum ribbons*. Nanoscale Res. Lett. **8**, 3, (2013)

[61] S. Mukhopadhyay, S. Gowtham, R. H. Scheicher, R. Pandey, S. P. Karna. *Theoretical study of physisorption of nucleobases on boron nitride nanotubes: a new class of hybrid nanobiomaterials*. Nanotechnology **21**, 165703, (2010)

[62] X. Zhong, S. Mukhopadhyay, S. Gowtham, R. Pandey, S. P. Karna. *Applicability of carbon and boron nitride nanotubes as biosensors: Effect of biomolecular adsorption on the transport properties of carbon and boron nitride nanotubes*. Appl. Phys. Lett. **102**, 133705, (2013)

[63] S. Grimme, J. Antony, S. Ehrlich, H. Krieg. *A consistent and accurate ab initio parametrization of density functional dispersion correction (DFT-D) for the 94 elements H-Pu*. J. Chem. Phys. **132**, 154104, (2010)

[64] J. Kohanoff. *Electronic structure calculations for solids and molecules: Theory and computational methods*. Cambridge University Press, New York, 2006.

[65] L. de la Peña. *Introducción a la Mecánica Cuántica*. Ediciones Científicas Universitarias, México, 2010.

[66] P. W. Langhoff, S. T. Epstein, M. Karplus. *Aspects of Time-Dependent Perturbation Theory* Rev. Mod. Phys. **44**, No. 3, (1972)

[67] A. L. Fetter, J. D. Walecka. *Quantum theory of many-particle systems*. McGraw-Hill, New York, 1971.

[68] D. J. Griffiths. *Introduction to Quantum Mechanics*. Prentice Hall, New Jersey, 1995.

[69] R. G. Parr, W. Yang. *Density-Functional Theory of atoms and molecules*. Oxford University Press, New York, 1989.

[70] P. Atkins, R. Friedman. *Molecular Quantum Mechanics*. Oxford University Press, New York, 2005.

[71] G. D. Mahan, K. R. Subbaswamy. *Local Density Theory of Polarizability*. Plenum Press, New York, 1990.

[72] A. D. Becke. *Density-functional thermochemistry. III. The role of exact exchange*. J. Chem. Phys. **98**, 5648, (1993)

[73] A. D. Becke. *Density-functional exchange-energy approximation with correct asymptotic behavior*. Phys. Rev. A **38**, 3098-3100, (1988)

[74] J. P. Perdew. *Electronic Structure of Solids*. Edited by P. Ziesche and H. Eschrig, Akademie Verlag, Berlin, 1991.

[75] J. P. Perdew, Y. Wang. *Accurate and simple analytic representation of the electron-gas correlation energy*. Phys. Rev. B **45**, 13244-13249, (1992)

[76] M. Dion, H. Rydberg, E. Schröder, D. C. Langreth, B. I. Lundqvist. *Van der Waals Density Functional for General Geometries*. Phys. Rev. Lett. **92**, 246401, (2004)

[77] A. Tkatchenko, M. Scheffler. *Accurate Molecular Van Der Waals Interactions from Ground-State Electron Density and Free-Atom Reference Data*. Phys. Rev. Lett. **102**, 073005, (2009)

[78] S. Grimme. *Accurate Description of van der Waals Complexes by Density Functional Theory Including Empirical Corrections*. J. Comput. Chem. **25**, 1463-1473, (2004)

[79] D. C. Langreth, B. I. Lundqvist, S. D. Chakarova-Käck, V. R. Cooper, M. Dion, P. Hyldgaard, A. Kelkkanen, J. Kleis, L. Kong, S. Li, P. G. Moses, E. Murray, A. Puzder, H. Rydberg, E. Schröder, T. Thonhauser. *A density functional for sparse matter*. J. Phys.: Condens. Matter **21**, 084203, (2009)

[80] Q. Wu, W. Yang. *Empirical correction to density functional theory for van der Waals interactions*. J. Chem. Phys. **116**, 515, (2002)

[81] U. Zimmerli, M. Parrinello, P. Koumoutsakos. *Dispersion corrections to density functionals for water aromatic interactions*. J. Chem. Phys. **120**, 2693, (2004)

[82] S. Grimme. *Semiempirical GGA-type density functional constructed with a long-range dispersion correction*. J. Comput. Chem. **27**, 1787-1799, (2006)

[83] F. Ortmann, F. Bechstedt, W. G. Schmidt. *Semiempirical van der Waals correction to the density functional description of solids and molecular structures*. Phys. Rev. B **73**, 205101, (2006)

[84] F. Maeder, W. Kutzelnigg. *Natural states of interacting systems and their use for the calculation of intermolecular forces: IV. Calculation of van der Waals coefficients between one- and two-valence-electron atoms in their ground states, as well as of polarizabilities, oscillator strength sums and related quantities, including correlation effects*. Chem. Phys. **42**, 95-112, (1979)

[85] A. Derevianko, W. R. Johnson, M. S. Safronova, J. F. Babb. *High-Precision Calculations of Dispersion Coefficients, Static Dipole Polarizabilities, and Atom-Wall Interaction Constants for Alkali-Metal Atoms*. Phys. Rev. Lett. **82**, 3589-3592, (1999)

[86] J. Mitroy, J.-Y. Zhang. *Long-range dispersion interactions. II. Alkali-metal and rare-gas atoms*. Phys. Rev. A **76**, 032706, (2007)

[87] S. Grimme, J. Antony, S. Ehrlich, H. Krieg. *A consistent and accurate ab initio parametrization of density functional dispersion correction (DFT-D) for the 94 elements H-Pu*. J. Chem. Phys. **132**, 154104, (2010)

[88] M. W. Schmidt, K. K. Baldridge, J. A. Boatz, S. T. Elbert, M. S. Gordon, J. H. Jensen, S. Koseki, N. Matsunaga, K. A. Nguyen, S. J. Su, T. L. Windus, M. Dupuis, J. A. Montgomery. *General Atomic and Molecular Electronic Structure System*. J. Comput. Chem **14**, 1347-1363, (1993)

[89] D. Le, A. Kara, E. Schröder, P. Hyldgaard, T. S Rahman. *Physisorption of nucleobases on graphene: a comparative van der Waals study*. J. Phys.: Condens. Matter **24**, 424210, (2012)

[90] B. Akdim, R. Pachter, X. Duan, W. W. Adams. *Comparative theoretical study of single-wall carbon and boron-nitride nanotubes*. Phys. Rev. B **67**, 245404, (2003)

[91] G. Y. Guo, J. C. Lin. *Systematic ab initio study of the optical properties of BN nanotubes*. Phys. Rev. B **71**, 165402, (2005)

[92] B. Akdim , S. N. Kim, R. R. Naik, B. Maruyama, M. J. Pender, R. Pachter. *Understanding effects of molecular adsorption at a single-wall boron nitride nanotube interface from density functional theory calculations*. Nanotechnology **20**, 355705, (2009)

[93] Z. Lu. *Synthesis and Characterization of Group 13 & 15 Complexes Supported by N,N'-Bidentate Ligands*. ProQuest Information and Learning Company, Texas, 2007

[94] S. F. Boys, F. Bernardi. *The calculation of small molecular interactions by the differences of separate total energies. Some procedures with reduced errors*. Mol. Phys. **19**, 553-566, (1970)

[95] B. Liu, A. D. McLean. *Accurate calculation of the attractive interaction of two ground state helium atoms*. J. Chem. Phys. **59**, 4557, (1973)

[96] S. S. Xantheas. *On the importance of the fragment relaxation energy terms in the estimation of the basis set superposition error correction to the intermolecular interaction energy*. J. Chem. Phys. **104**, 8821, (1996)